10-19-2015

Coating Prospects in Corrosion Prevention of Aluminized Steel and Its Coupling with Magnesium

Fuyan Sun
University of Windsor

Coating Prospects in Corrosion Prevention of Aluminized Steel and Its Coupling with Magnesium

By

Fuyan Sun

A Thesis
Submitted to the Faculty of Graduate Studies
through the Department of Mechanical, Automotive and Materials Engineering
in Partial Fulfillment of the Requirements for
the Degree of Master of Applied Science
at the University of Windsor

Windsor, Ontario, Canada

2015

Coating prospects in corrosion prevention of aluminized steel and its coupling with magnesium

by

Fuyan Sun

APPROVED BY:

_____
Jichang Wang
Department of Chemistry&Biochemistry

_____
J. Sokolowski
Department of Mechanical, Automotive and Materials Engineering

_____
Xueyuan Nie, Advisor
Department of Mechanical, Automotive and Materials Engineering

16 September 2015

DECLARATION OF ORIGINALITY

I hereby certify that I am the sole author of this thesis and that no part of this thesis has been published or submitted for publication.

I certify that, to the best of my knowledge, my thesis does not infringe upon anyone's copyright nor violate any proprietary rights and that any ideas, techniques, quotations, or any other material from the work of other people included in my thesis, published or otherwise, are fully acknowledged in accordance with the standard referencing practices. Furthermore, to the extent that I have included copyrighted material that surpasses the bounds of fair dealing within the meaning of the Canada Copyright Act, I certify that I have obtained a written permission from the copyright owner(s) to include such material(s) in my thesis and have included copies of such copyright clearances to my appendix.

I declare that this is a true copy of my thesis, including any final revisions, as approved by my thesis committee and the Graduate Studies office, and that this thesis has not been submitted for a higher degree to any other University or Institution.

ABSTRACT

In this study, a plasma electrolytic oxidation (PEO) process was used to form oxide coating on aluminized steel, heated aluminized steel and magnesium. A potentiodynamic polarization corrosion test was employed to investigate the general corrosion properties. Galvanic corrosion of steel samples and magnesium samples was studied by zero resistance ammeter (ZRA) tests and boiling tests. Scanning electron microscopy (SEM) and EDS were used to investigate the coating microstructure and the coating/substrate interface. In general, the PEO coatings on all three substrate can help prevent general corrosion. 6-min coated magnesium with unipolar current mode performs best in most galvanic couplings for preventing both general corrosion and galvanic corrosion. Factors which could influence galvanic corrosion behaviors of tested samples were discussed based on area ratios of anode/cathode and cell potential driving force during the ZRA corrosion tests and boiling tests.

DEDICATION

To My Parents,

Bing Sun and Caixiu Liu

For their endless love and devotion

ACKNOWLEDGEMENTS

TABLE OF CONTENTS

VIII

LIST OF TABLES

LIST OF FIGURES

XIV

XVII

Chapter 1: INTRODUCTION

1.1 Motivation

Automotive manufacturers are constantly complying with more and more restrictive environmental rules. The automotive emission is one of the most important reasons for the increased frequency of severe weather conditions. To decrease the greenhouse emission, car industries are increasingly interested in employing lightweight materials such as magnesium and aluminized steel to reduce vehicles weight and fuel consumption. Also, high strength steel with good formability can also decrease the weight of automotive in terms of the same suffering strength.

Magnesium has abundant natural resources with 2 % weight fraction of earth crust. In order to reduce the weight of cars, the magnesium is widely used in different vehicle components. It is first introduced by the Volkswagen for transmission part. The further application extends to the drive train, steering wheel part to replace the cast iron/steel parts. However, the limits on corrosion behavior, mechanical strength and other performance are still the challenges in engineering design. There is thus the need for a more corrosive resistant coating on magnesium to improve the corrosion behavior [1-3].

Aluminized steel has been widely used, since its introduction to industry, as components in vehicles, bridges, pressure containers, and house appliances [4, 5]. The hot dipped aluminum coating on steel provides long-term galvanic protection against pitting corrosion and long-term protection against cosmetic red rusting. In auto industry, aluminized advanced high strength steel (AHSS) are used due to the weight reduction. The Al-Si alloyed surface layer of aluminized AHSS is utilized to prevent the scaling during hot stamping. However, aluminized steel can pits

gradually after exposure to moist salt after cycles of corrosion. In case of corrosion protection, protective coating is a good idea.

Galvanic corrosion is an enhanced corrosion between two or more electrically connected dissimilar metals [6], where the more active one acts as anode and corrodes and the less active one is cathode [7]. The corrosion rate of anodic material will be increased and the cathodic material will be protected. As for aluminized AHSS, the Al surface layer would protect the base material steel from corrosion. Besides the use of AHSS for weight reduction, light alloys (magnesium alloys, for instance) have also found increasingly applications in vehicles. On one hand, prevention of light alloys from general corrosion by using a coating technology is usually necessary. On the other hand, there is a big chance for a coupling of aluminized steel/aluminized AHSS with uncoated or coated magnesium (Mg) alloy that cannot be avoided in vehicle assembly. Therefore, study on surface treatment of those alloys for corrosion prevention is critical.

By using plasma electrolytic oxidation coating method, the abilities of magnesium, aluminized steel and aluminized AHSS to bear corrosion can be increased. Combining electrochemical oxidation with plasma discharge in electrolyte, PEO (plasma electrolytic oxidation) technique can produce ceramic coatings with properties such as high hardness, wear resistance, corrosion resistance and thermal protection [8].

In this study, the substrate materials are aluminized steel, aluminized AHSS and magnesium. PEO method was employed for coating preparations on those substrates. In particular, two current modes (unipolar and bipolar) were applied to coat magnesium. The corrosion resistance was determined by potentiodynamic

2

polarization test. Surface morphology and cross sectional structures of coatings were characterized by scanning electron microscopy (SEM). The coating prospects of aluminized steel, aluminized AHSS and magnesium in galvanic couples were investigated by ZRA corrosion tests and boiling tests.

1.2 Objectives and contents of this study.

The objectives of this study are to:

1.   Produce oxide coatings on Mg, aluminized steel and aluminized AHSS using Plasma Electrolytic Oxidation (PEO) process

2.   Inquire proper experiment conditions of treatment time for aluminized steel coating process and magnesium coating process.

3.   Research on the prevention of aluminized steel/Mg coupling and high strength steel coupling due to the galvanic corrosion.

1.3 Organization of the thesis

This thesis includes five chapters. In Chapter 1, the application of magnesium, aluminized steel and aluminized AHSS are introduced. The PEO coatings are deposited in order to increase the corrosion behavior in both general corrosion and galvanic corrosion.

Chapter 2 gives the literature review of light weight metal applications in automotive industry. The corrosion types of light weight metal in applications are illustrated. The theory of plasma electrolytic oxidation (PEO) deposition is also given in this chapter.

Chapter 3 describes the experimental procedures and characterization instrumentation. In chapter 4, experimental results and analysis are given. For the conclusions and future work, the chapter 5 gives a detailed summary.

Chapter 2: LITERATURE REVIEW

2.1 Lightweight metal applications in automotive industry

The concerns about global warming and fuel consumptions have a significant influence on the choice of materials. For example, US government issues a policy [9] to reduce vehicle exhaust emissions to boost fuel economy. The vehicle companies modify conventional engine efficiency and design new power system and hybrid system to decrease automotive weight. Electric vehicles priority in Chinese government give a chance to decrease its dependence on overseas oil, develop air condition by forbidding sectional transportation, and positively join the global industrial world with developed economy [10]. Electric vehicles and light weight vehicles can serve as two possible solutions to solve the environmental problems. So the light weight material is inevitably utilized in the worldwide. In addition, with the development of vehicle market, the new models are designed with good performance, high safety and extreme luxury to meet the demand of consumers. Safety settings such as air bags and anti-break systems increase weight gain to the automotive. This problem can also be solved by utilizing lightweight materials, such as magnesium and aluminum that obtain the lightest density among all industrial raw materials (ρ_{Al}=2.7 g cm^{-3}, ρ_{Mg}=1.7 g cm^{-3}). A lightweight design can also be attained by substituting the conventional material to high-strength steel and other composites [11].

2.1.1 Aluminum application in automotive industry

Due to the light weight, relatively easy fabrication, good corrosion performance and attractive mechanical properties, aluminum usage in vehicle applications has increased 28% in 2015 over 2012 [12]. The use of aluminum begins with their spectacular development into the aerospace industry. And its spreading has been

classified as: 1) Power train (engine, fuel system, liquid lines):25 components analysed in cylinder head and engine block, radiators and transmission housings. 2) Chassis and suspension (cradle, axle): 17 components analysed in wheels, steering systems and suspension arms. 3) Car body (hoods, doors, bumpers, wings and interiors):20 components analysed in doors and bonnets, front structure and bumper beams [13]. The aluminum consumption of different systems of year 2015 in North America is estimated in the figure 2.1.

There are two main alloy systems in vehicle application: Al-Mg (AA5xxx) and the age-hardened Al-Mg-Si (AA6xxx) [14]. Because of good forming behavior, 5xxx Al-Mg alloys is well established in chassis and various structural applications. Also they appear in sheet panels but seldom in exterior parts. 6xxx Al-Mg-Si is mostly used in exterior panel since it can meet the requirements for surface appearance. The other alloying additions such as Mn, has a beneficial effect on the mechanical properties and is added mainly to regulator grain size by forming sub-micrometer-sized particles [15]. Fe addition element in aluminum can have a negative effect. Fe-added alloys have low solubility so block the forming of constituent particle during eutectic solidification.

The tensile strength of aluminum alloys are generally in range of 70-700 MPa. In extrusion process it can reach to the range of 150 – 300 MPa. Aluminum has enough toughness at low temperature which is different from steel alloys. To the contrary, the strength of aluminum will descend when temperature increases. At even high temperature, the weakening needs to be considered in case of inferior quality of aluminum products. Metal forming of aluminum alloys is mainly achieved by extrusion and casting. In early years, aluminum space frame and complex sub-structures have been developed using aluminum extrusions. Aluminum can adapt to

complex design and functional integration for cost-effective mass production. For example, medium strength 6xxx and high strength 7xxx age-hardening alloys are utilized because of the quenching needed in extrusion process.

Most of the aluminum components are using casting method, such as engine block, engine head and other vehicle body parts. Cast iron engine part is being substituted by the aluminum engine. Although cast iron diesel engine has high strength and durability, the needs for low exhaust emission push the growth of aluminum engine. New casting techniques also achieve this development [13].
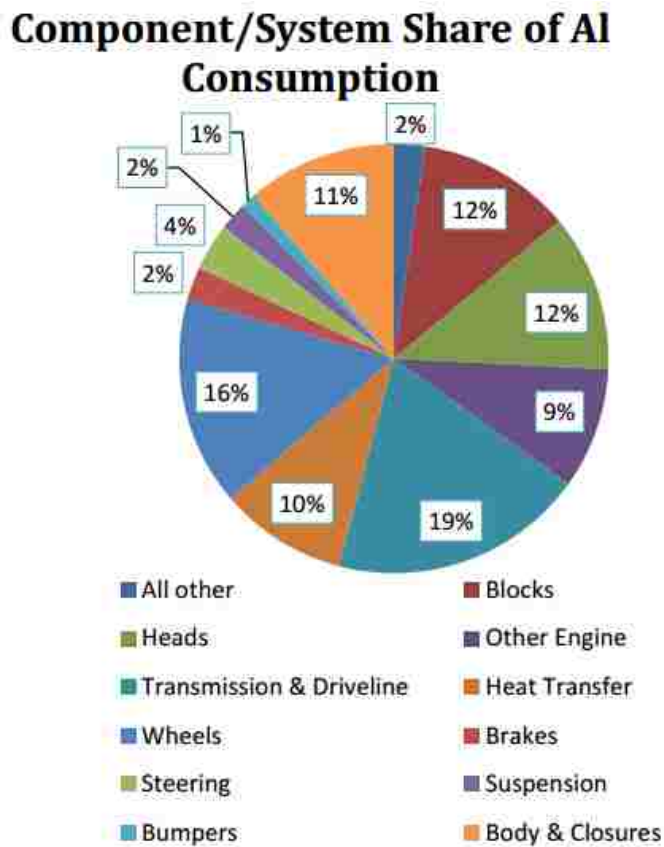
Figure 2.1 Expected component/system share of aluminum consumption in North America in 2015 [4].

2.1.2 Magnesium applications in automotive industry

The increasing need for improved fuel economy has offered a significant interest in lightweight vehicle structures. This idea can be achieved by the reasonable structure design and direct weight decrease. Considering the lightness of magnesium, it is supposed to substitute steel in automotive application [16]. The first magnesium age started after the Second World War with the application of air-cooled engines and gearboxes. At that time, company like Volkswagen commit itself to the entire technical design with lightweight magnesium [17].

The use of magnesium can decrease the average weight of the automotive. More and more aluminum and steel components are replaced by the magnesium in the research center of international companies. Audi, Ford, Fiat Jaquar and Kia are just small part of these companies (Figure 2.2). Magnesium is most used in lift gate panel, instrument panel, gear box, driving chains and seat frames. For example, the reinvented Ford Explorer, the 2011 North American Truck of the Year, uses magnesium seat frames for its third-row passenger seats. Strategic magnesium use supports Ford Motor Company's commitment to vehicle quality, reliability, fuel efficiency, safety, smart design, and affordability. Strategic use of lightweight and down-gauged material allows a vehicle's powertrain to be smaller and more fuel-efficient. Combining magnesium with aluminum for the MKT lift gate's panels instead of steel saves 22 pounds in vehicle weight. When coupled with other weight-saving measures, re-matching the vehicle with a smaller powertrain – known as right-sizing of power to weight -- is a key factor in achieving greater fuel economy [18].

Magnesium and its alloys can be handled either through solid or liquid phase. Solid phase processing is not very popular. It is because that the high cost in the process, brittleness and inferior toughness. Liquid phase process includes squeeze casting, sand casting and metal casting.

Figure 2.2 Automotive products use lightweight magnesium structures to decrease fuel exhaustion. Shown: 1) Acura ZDX, 2) Jeep Grand Cherokee, 3) Chevrolet Corvette Z06, 4) Ford Explorer and 5) Volkswagen Golf [18].

Most of the magnesium source will be suffer die casting. The low cost of the casting process and goo quality of production make it most common in casting of magnesium. Die casting utilize the narrow opening to squeeze the molten magnesium in to a specified mold with a proper speed. The operation process pressure can be high to 1000MPa in solidification [19]. The advantage of process pressure in stage of solidification will decrease the porosity and increase the integrity of the magnesium products. Molten magnesium is cast by die casting to produce thin shape products. The die casting can provide good strength, simple machining process and high quality for magnesium products. The mechanical properties are directly influenced by the thickness of product. The metal waste can reach half of raw material will be recycled by the runner system [20-24]. Figure 2.3 shows the schematics of die casting [25].
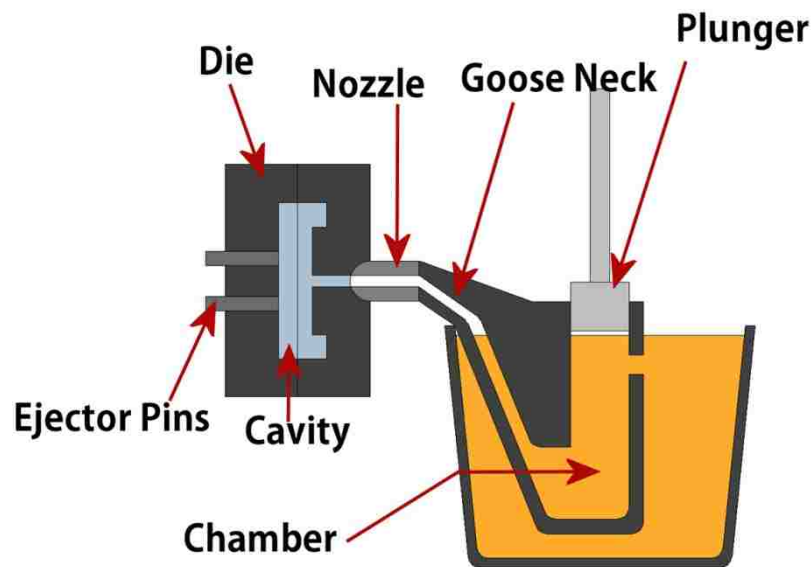
Figure 2.3 Schematics of hot chamber die casting [25].

2.1.3 Advanced high strength steel (AHSS) application in automotive industry

With the increasing requirements of customer safety, car behavior and natural resources economy, there is a strong comparison between low density metal and steel. To face the challenge, higher strength steel is developed rapidly in steel industry. The ductility decreases with strength in conventional steel, but the formability and high strength can be both derived in AHSS. As a result, AHSS is becoming a vital part in industrial applications. The AHSS can be classified as the following types: dual phase (DP), complex phase (CP), transformation induced plasticity (TRIP) and martensitic steel (MART). The classification involves ultimate tensile strength (UTS) and yield strength (YS) and summarized as XX aaa/ bbb, where XX is the classification of steel, aaa represents minimum YS and bbb is minimum UTS. [26].

The mostly used AHSSs insists of dual phase (DP), transformation induced plasticity (TRIP). The substrate microstructure is ferrite which is surrounded by martensite which is shown in figure 2.4. The martensite is derived from the quick cooling technique of austenite. The amount of martensite is the key factor that affects

10

the mechanical properties of DP steels. It will increase the tensile strength and hardness of DP, but reduces the ductility. DP steels can show tensile strengths that in a range of 450-1200 Mpa and elongation from 20% to 3% by surge the volume of martensite [27].
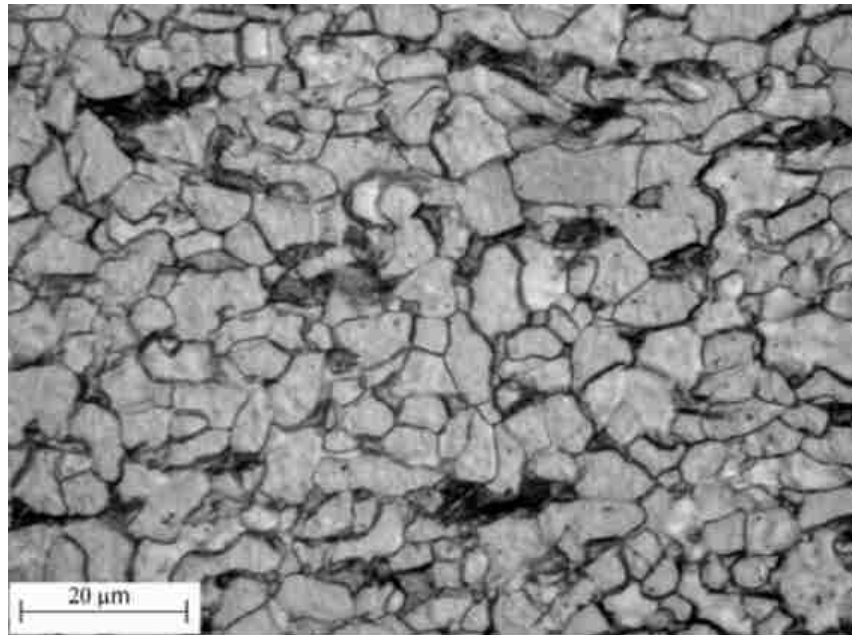
Figure 2.4 SEM picture of dual-phase steel microstructure [26].

The alloying elements in DP steels can affect the strength properties. For example, Mn (1.5%-2.5%) is the austenite stabilizer and can retard ferrite formation. Si can promote the transformation of ferrites. Cr and Mo are the perfect inhibitor of pearlite and banite. Element V (0.06%) is beneficial to precipitation and microstructure refining. Nb can also refine microstructure and promote ferrite transformation from non-recrystallized austenite.

The most common producing method of DP steels is by cold rolling of low alloy steels and then continuous annealing line to form the martensite from austenite/ferrite phase. The austenite phase will change to the martensite through quenching which provides proper hardenability and proper cooling rate. This chain production method

can form microstructure consisting ferrite surrounded by imbedded hard particles. A schematic picture of production layout is presented in figure 2.5.
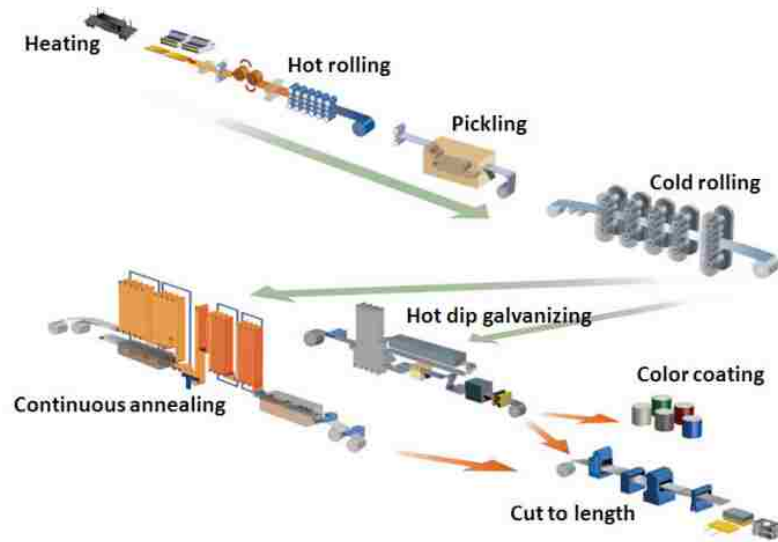
Figure 2.5 Schematic picture of the production layout [29].

2.2 Corrosion characteristics of aluminized steel

Corrosion prevention of drainage pipes is a vital part in highway structures. Durable metallic materials such as aluminum alloys and galvanized steel are widely used in the drainage pipes design. Recently, aluminized steel is increasingly being popular. In addition, aluminized steel bolts are utilized in connection parts between engine head cover and engine head. Although the alumina and galvanized layer can help prevent corrosion in the natural environment, it is still essential to predict corrosion

2.2.1 Manufacture of aluminized steel

In the past decades, different aluminizing methods have been widely utilized. The protection process is different but all are followed by the hot-dipping stage. The steel to be hot-dipped is degreased by alkali cleaning or by heating at 450-600 ℃. Water

rinsing, pickling is followed in the preheatment process. The surface of steel strips is cleaned to obtain a smooth surface for adherence. The hot-dipping process is operated in a closed environment at above 700 ℃. Finally, line annealing of steel strips decide the aluminum coating thickness. According to the ASTM A929 and ASSHTO M274 standard procedures, there is a minimum coating weight of 1 oz/ft^2 which corresponds to a minimum coating thickness of up 40μm and a minimum yield and tensile strength of about 228 MPa and 310 MPa, respectively[30-34].

2.2.2 Morphology of intermetallic layer in hot-dip aluminized steels

Intermetallic Fe_2Al_5 will form in the aluminized layer above the substrate during hot dip aluminizing [35]. With the high temperature diffusion, Al_2O_3 layer gradually appear on the surface of substrate steel. And the main content of the layer between this Al_2O_3 layer and substrate steel is Fe_2Al_5. X-ray diffraction and EDX analysis in figure 2.6 prove that the dominant phase of the intermetallic layer is Fe_2Al_5 [36].

SEM image of surface morphology is described in Figure 2.7. Fe–Al intermetallic grains cultivate gradually to the direction of steel substrate and the needle grains grow in the top aluminum layer [36]. Fe_2Al_5 can diffuse into multi-sub layers with accumulating aluminum to the steel substrate [37]. Since this orthogonal-lattice-structural layer of Fe_2Al_5 has high hardness and unstable structure (caused by cavities and cracks), it is easier to scale off under external strength [38].
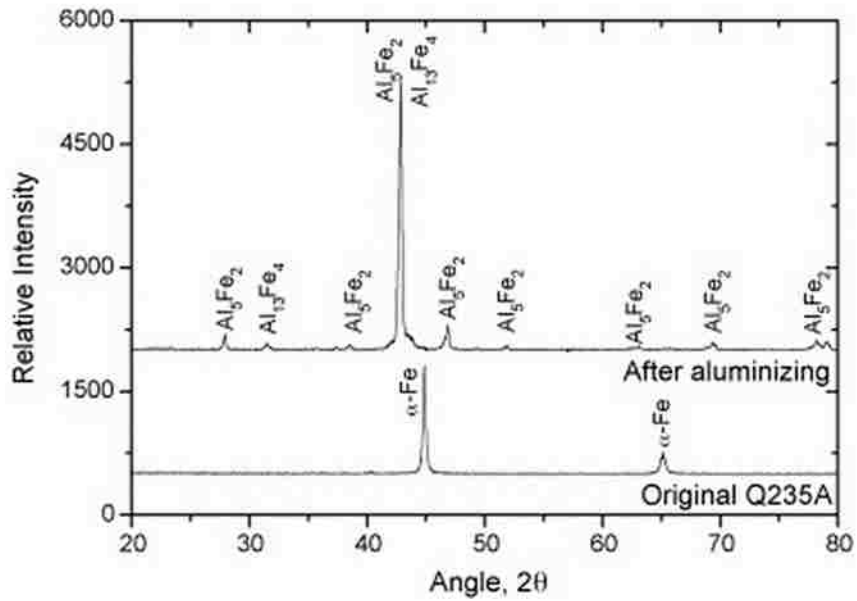
Figure 2.6 X-ray diffraction patterns of the Q235A steel [36].
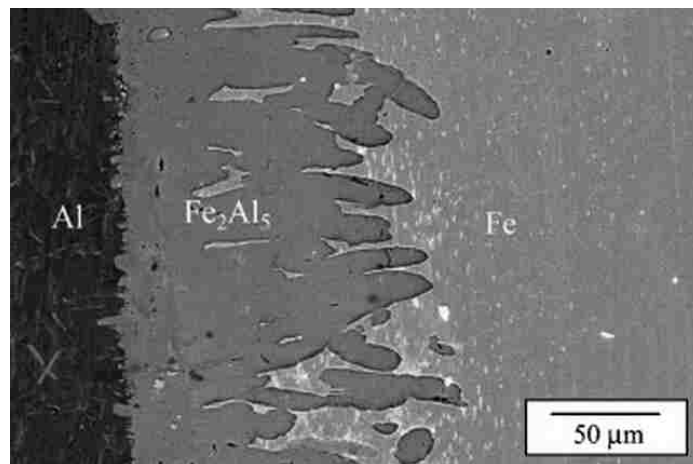
Figure 2.7 Cross section SEM image of the aluminized sample after pre-treatment at 650 ℃ for half an hour [36].

There is a recent review of aluminized steel corrosion conducted by Caseres, L. (2007). Highlights of that work can be summarized as followed. The thin passive oxide aluminum layer can decrease the oxidation rate of the inner metal substrate. When contacted with water, the outside layer can become layer with content of

14

$Al_2O_3 \cdot 3H_2O$. In spite of extreme acid or alkaline solution, aluminum tends to be covered by a protective oxide layer when the pH is between 4 and 8.5. Since a small current can be found during metal polarization, Hunter and Fowle (1956), Lee and Pyun (1999) supposed that there were two layers composing the oxide film. Inner oxide layer close to substrate metal has compacted amorphous structure. Outside layer is a thicker and more permeable. However, if the pH value of aqueous solution is beyond 8.5, the protective formed oxide layer will dissolve. And the extremely acidic environment will cause the decomposition of oxide layer.

The thickness of aluminum and intermetallic layers in aluminized steel are dependent on time and temperature. Deqing Wang (2003) did aluminizing process on the steel alloy substrate. The melt aluminum was kept at different dipping temperatures [37]. Then the steel substrate was immerged into the molten aluminum for different holding time. Figure 2.8 shows the temperature and time effects on aluminum layer. As the holding time increases, the thickness of pure aluminum layer is reduced at each different dipping temperature. When time is kept constant, the thickness of pure aluminum layer decreases with the increase in dipping temperature. After 30 minutes, time and temperature will not affect the thickness.

However, the thickness of intermetallic layer in increased when temperature and holding time ascend. It is suggested that diffusion aluminum atoms will rise up when there is an increase in temperature and time.
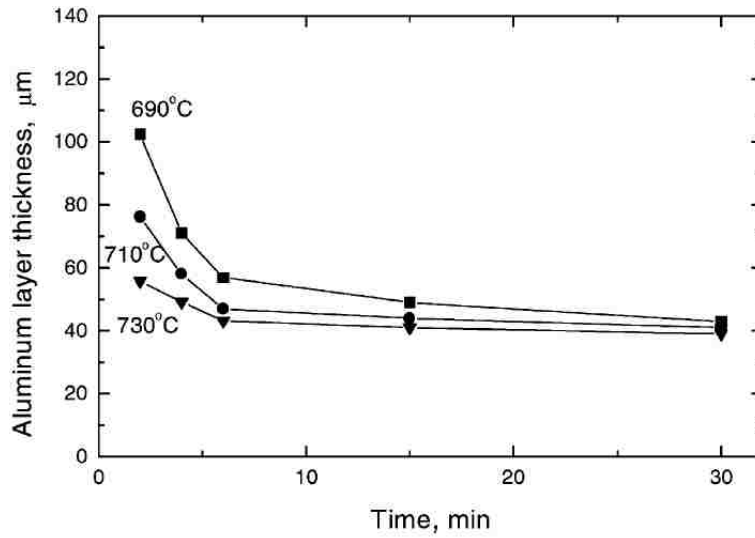
Figure 2.8 Influences of dipping temperature and time on the thickness of pure aluminum layer [37].
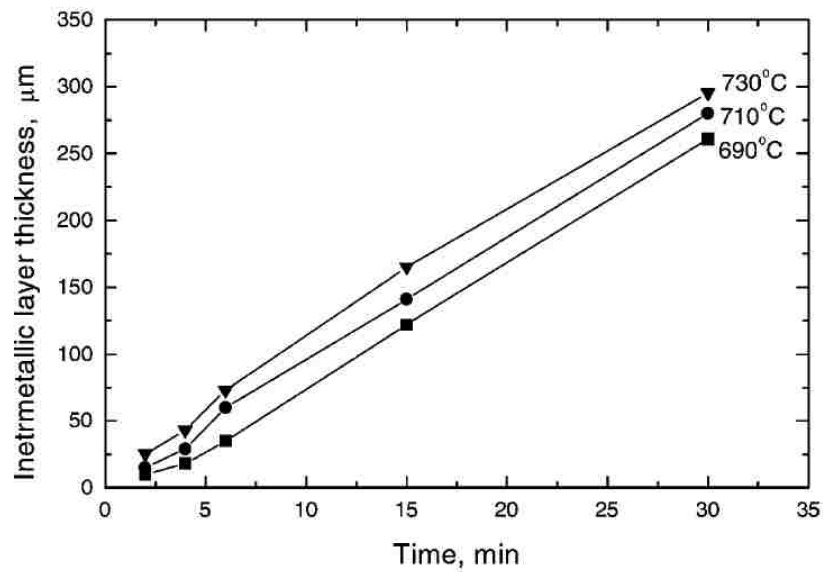
Figure 2.9 Influences of hot-dipping temperature and time on the thickness of intermetallic layer [37].

2.2.3 Corrosion behavior of pure aluminum layer on aluminized steel

Aluminum is a thermodynamic reactive metal according to its position in electrode force series. But due to barrier oxide film, aluminum owe a high corrosion

16

resistance and to be used primarily in corrosive environment. In the ambient temperature, the oxide film is 5nm and if removed the corrosion will take place. In addition due to the aluminum present as the alloy form mostly, electrochemical corrosion will occur because of the potential difference between additives and aluminum [39].

2.2.4 Pitting corrosion of aluminum layer

Pitting always forms at some heterogeneities of metal surface such as grain boundaries, flaws, inclusions and surface dislocations. In general, the pitting process of aluminized steel can be summarized as below. At first, the pitting occurs outside the passive film and gradually moves into the passive film. There are no obvious microscopic changes in it. Then the metastable pits initiate and finally result in the stable pitting growth [40]. The passive film can be weakened by intermediates. Galvanic can form between aluminum matrix and intermetallic layers.

Interaction of chloride anions with passive film have been analysed by different technique. The adsorption energy of metal surface differs from site by site since of the metal defects. Berzing made research about the chloride adsorption. He concluded that chloride concentration (Cl) and time can affect chloride adsorption. In equation $\log \omega \text{Cl} = 0.64(\log(Cl) + \log t) - 7.8$, the unit of ωCl, (Cl) and t (time) are g cm^{-2}, mol^{-1} and min respectively [41]. And chloride adsorption increases linearly with the potential. Aluminum chloride and aluminum oxychlorides are two main pit's salts. There are following sequence of reactions.

$\text{Al}^{3+} + \text{H}_2\text{O}\text{----}\text{H}^+ + \text{Al (OH)}^{2+}$

$\text{Al (OH)}^{2+} + \text{Cl}\text{-----} \text{Al (OH) Cl}^+$

Al (OH) Cl$^+$ +H$_2$O----Al (OH) $_{2Cl}$+ H$^+$
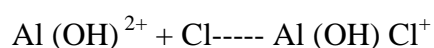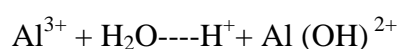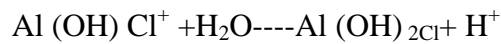
2.3 Corrosion of magnesium

Magnesium alloys are widely used in the electronics, vehicles and aerospace industries. The automotive application made by magnesium is becoming an important research topic. For example, Volvo Company had a project called light component project in 1980. Magnesium is the most anodic or active metal in the electrode series [42], so the major challenge for mass production of automotive components is galvanic corrosion. Although the corrosion can be avoided by blocking direct electrical contact between galvanic couples, the indirect contacts are inevitable in the component design due to the electrical and mechanical demands.

The alloying element of magnesium alloys can also affect the corrosion behaviors. For example, the corrosion resistance ranking is ZK60> AM60> AZ31> AZ91 [43].The results indicate that the corrosion resistance is related to alloying elements and micro-grains of magnesium alloys. The galvanic corrosion and general corrosion are the major pattern of erosion. The micro-galvanic cell rate in AZ31 is lower than that in AZ91. The AlMnFe caused by manganese element can reduce the Fe content in alloy matrix. This is the reason that corrosion resistance of AM60 is higher than that of AZ series. The ability of zirconium for refining crystals and purifying the compounds allow ZK60 having the highest corrosion resistance. In general, the corrosion resistances of magnesium alloy are relying on the alloying elements and impurity contents (β phase). Effect of aluminum content is analysed by constant research papers. Lunder et al [44] found that corrosion resistance of magnesium alloys will rise up when the mass content of aluminum exceeded 8%. Other researcher such as Hehmann et al [45] mass fraction range from 9.6% to 23.4% of aluminum is most

favourable to magnesium alloys. Likely, there are many different versions about β phase effect on alloys. On the one side, most considered it as cathode in the micro-galvanic couples so it will increase the corrosion of magnesium alloys, but on the other side, the β phase will form a barrier inside metal layers to resist corrosion. And the particle size, mass fraction and distribution of β phase closely affected the magnesium alloys [46].

2.4 Galvanic corrosion

2.4.1 Galvanic corrosion between aluminized steel and magnesium

In general aluminum won't dissolve except put in highly acidic or alkaline solutions. But when meet phosphoric acid or sodium hydroxide in natural environment, aluminum will be soluble at a steady rate. Dissolution is rare in pure aluminum. However, extremely alloyed heat-treatment material such as aluminized steel always show galvanic corrosion. If cross-sections of alloys are damaged, atom exchange between multi-layers outside the substrate steel.

Galvanic corrosion occurs in most natural waters. Evidently, aluminum and its alloy supposed to be anodes when contact with other metals. In table 2.1, only magnesium and zinc are more anodic and can protect aluminum when there is a galvanic cell. The most inactive metals are at top and most active metals are at the bottom. The galvanic series is set according to the electrode potential in salt corrosive solution. Since aluminum alloys are in the different position of electrode series. When the construction materials are all aluminum alloys, it's important to prevent galvanic corrosion.

There are four factors that can influence the rate of galvanic corrosion: difference of corrosion resistance between two metals; gap of electrode potential between galvanic combinations; anode-cathode explosion area ratio and polarization extend of two dissimilar metals. For example, the electrode gap between stainless steel and aluminum is greater than that between copper and aluminum but the galvanic corrosion on aluminum caused by steel is inevitable compared to the influence on aluminum caused by copper. This phenomenon is due to the polarization of steel-aluminum couple. Polarization means that when contact with electrolysis, the electrode will change its value. The anodic electrode will become nobler, while the cathode will become more active. Polarization often accomplished by formation of a film on the electrode surface.

Table 2.1 Galvanic series of metals exposed to seawater [47].
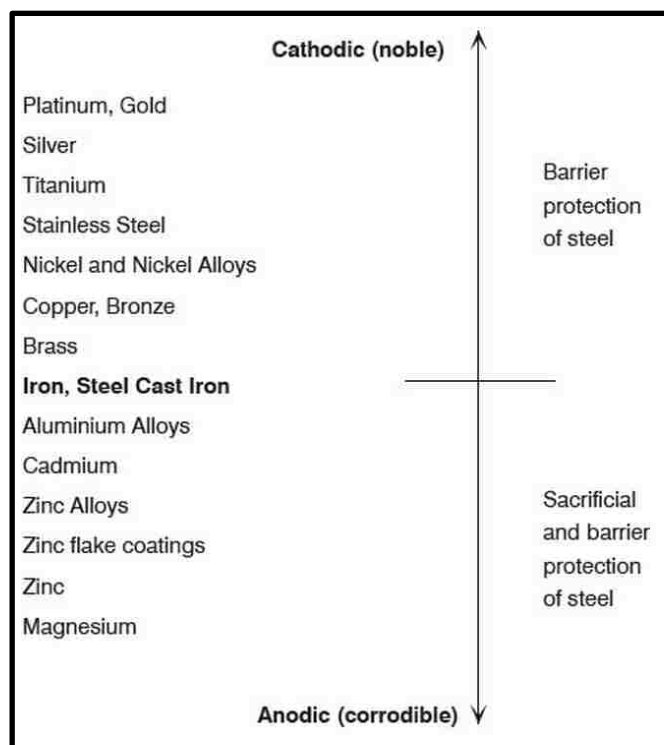
In addition, the galvanic rate between magnesium alloys and other metals is still important too. Song [48] found that the corrosion rate was closely related to the contact time, anode/cathode ratio, insulating spacer thickness and corrosion products. Galvanic corrosion increases with contact time when connected with different metals (zinc, steel 4150 and Al380). When ratio of anode/cathode area decreases, the corrosion rate will increase. Coupling type of large cathode material (steel, aluminum and zinc) and small magnesium should be avoided. Otherwise, severe corrosion will happen. The reaction products can also influence the galvanic corrosion. Magnesium ion forms around the anode and magnesium dissolution produces $Mg(OH)_2$ with the hydrogen. The solution is alkaline because of $Mg(OH)_2$.

This research focuses the galvanic corrosion between aluminized steel and magnesium. Song [48] operated a measuring test according to specifically designed sheets. The ratio of anode/cathode area, circuit current density and effects of reaction products are all mentioned due to the originally designed test. Liu [49] considered that polishing process with water will increase the galvanic corrosion in the joint of magnesium alloy and aluminum alloy. The X-ray spectroscopy and scanning electron microscopy are used to help analysed the cross-section between aluminum and magnesium.

2.4.2 Galvanic corrosion protection

To protect aluminum from galvanic corrosion, the ratio of anode/cathode area, connected metal potential and circuit current are being analysed. To reduce the corrosion of aluminum, the more inactive metal should be avoided. When the automotive manufacture needs specific galvanic couples, the high ratio of anode/cathode is preferable [50]. The ratio can be increased by make coatings on

21

cathodic metal or both two electrode metal. Also the oxidizing agents will accelerate the corrosion rate, and removing them is beneficial of prevention [51].

Sometimes cathodic protection can be a kind of prevention method. Here are several examples: 1. the ford mkt lift gate is made of magnesium and tiny connecting bolts are steel. The galvanic corrosion between magnesium and steel can be eliminated by putting thin film or coating on steel (aluminum layer or oxide coating). 2. Some engine head are made of magnesium but block is aluminum. To add coating on both magnesium and aluminum can prevent general corrosion and galvanic corrosion. Since the coating on two electrode or cathodic electrode will increase the area ratio of anode/cathode. The magnesium is to be the anode because of the higher electrode potential.

Surface treatment is also widely used in material industry. The zinc-coated aluminum alloy is the result of diffusion cladding. The whole procedure is to deposit zinc on the surface of aluminum then form the zinc-coated aluminum by passing specific solution. Thermal spray is utilized to form thin coating on the surface of aluminum. Also aluminum can also be an anodic protective metal to be deposited on the nobler metal. Conventional aluminized steel are produced by putting zinc or pure aluminum on the surface of steel. This aluminized steel possesses the strength of steel and corrosion resistance of aluminum [52-55].

2.5 The choice of substrate material.

With the increasing requirements of customer safety, car behavior and natural resources economy, there is a strong need for low density metal and high strength steel. To face the challenge, magnesium and higher strength steel are developed rapidly in steel industry. For magnesium, many large automotive companies have

already replaced steel and aluminum with magnesium in various parts of their products due to its light weight. For AHSS, although ductility decreases with the increase of tensile strength in conventional steel, formability and high strength can be both derived in advanced high strength steel (AHSS).

Why do we choose to add Al layer onto the top of steel and AHSS? Since in the austenitization process of hot stamping, there will be oxide scale on the surface of steel when the steel contacts with air. The Al-Si protective layer can prevent the scale formation during the direct hot stamping operation. This metallic coating is formed during the continuous hot-dip process. The interface area of the coated blank will diffuse to the surface layer during heating. Al-Si surface coating has a lower melting point (600 ℃) than the substrate Fe, and that Fe-Al diffusion will help prevent the melting of surface. And for a typical 950℃ direct hot stamping, a layer consists of Fe and Al is formed between surface Al-silicon layer and Fe substrate. In case of the break of coating in the cold pre-forming process in in direct coating, the Al-Si layer is not suitable for indirect hot stamping process. Figure 2.10 shows two kinds of hot stamping process. The difference between them is that metal shape is formed before austenitization [56].

There are also other coatings for the protection of steel. For example, Zinc layer can provide cathodic protection for the steel sheet. The x-tec coating is suitable for both direct and indirect hot stamping process. In this coating, aluminum is blended with organic and inorganic material to form a 7μm layer. The latest coating method is using oil to prevent oxidation.
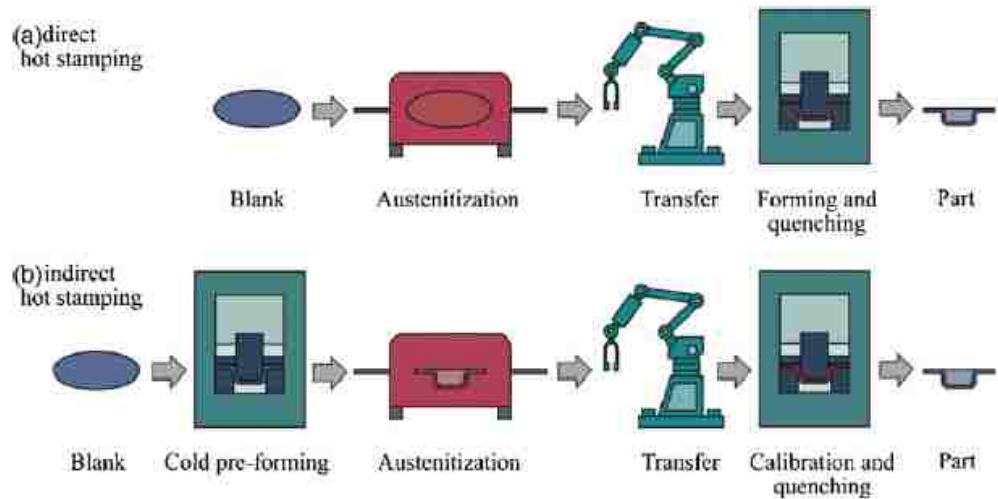
Figure 2.10 Basic hot stamping process illustration: (a) direct hot stamping, (b) indirect hot stamping [56].

2.6 Coating method review

2.6.1 Chemical vapor deposition (CVD) introduction

The difference between Chemical vapor deposition (CVD) and PVD is the coating process they utilize. In CVD, the precursor gases are carried to a reaction chamber. The reaction or decomposition will happen when the carrier gases meet the substrate surface and finally deposit a coating on material. Figure 2.11 shows a working process of CVD. Here takes the metal chemical vapor deposition as an example. Advanced CVD processes utilize of photons, ions and plasmas. There are a variety of CVD processes such as plasma assisted chemical vapour deposition (PACVD) and laser chemical vapour deposition (LCVD). CVD has a variety of significant advantages. One of the primary benefits is that CVD films can be quite conformal. The porous structure will be highly eliminated. Another advantage is that the applying material can be in a wide range and can be deposited in high purity. This

reduces the impurity extent. In addition, CVD don't need specific reaction situation such as a high vacuum condition.
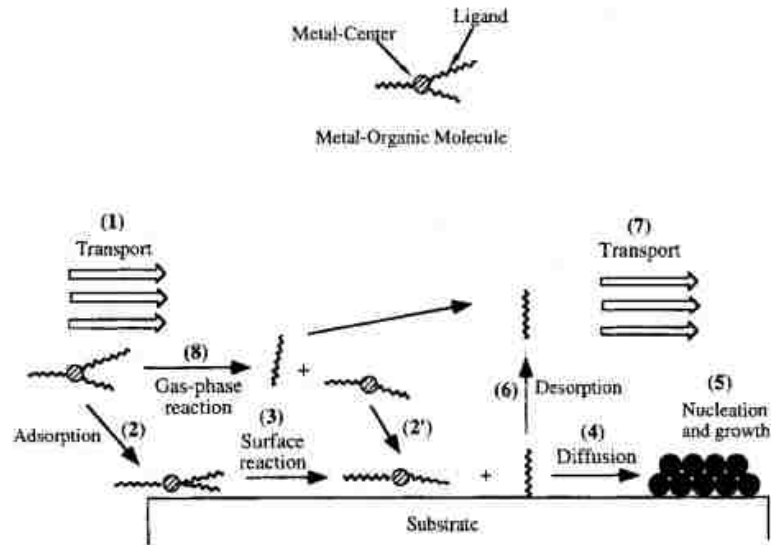
Figure 2.11 Important steps involved in metal CVD [57].

2.6.2 Physical vapor deposition (PVD) introduction

Physical vapor deposition (PVD) is widespread in coating industry. Thin films of ceramic, metal and polymer are deposited onto a wide range of materials. And advanced PVD methods are created due to the high demand for high corrosion resistance, high hardness, low friction and specific conductive properties [58]. PVD methods include evaporation deposition, sputter deposition, arc deposition, ion plating and hybrid PVD process. Several PVD processing method are depicted in Figure 2. 12. Deposition material first change to its vapor phase. The transportation of vapor species to substrate produces the plasma with or without collision between atoms and molecules. Final process includes the condensation of the vapour species and the formation of films. Critical factors are nucleation and grain growth [59].

In this research, the plasma electrolytic oxidation (also known as the micro arc oxidation) will be used to produce coating on aluminized steel, magnesium and advanced high strength steel. The details about plasma electrolytic oxidation coating method will be illustrated in next part.
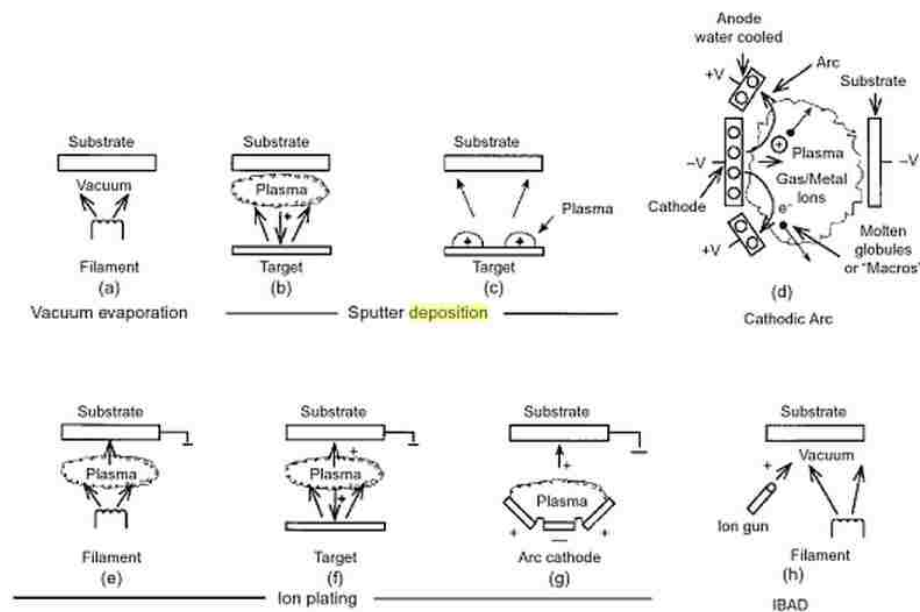
Figure 2.12: PVD processing techniques: (a) vacuum fading, (b) and (c) sputter deposition in a plasma situation, (d) sputter deposition in a vacuum, (e) ion plating in a plasma situation with a thermal evaporation basis, (f) ion plating with a popping basis, (g) ion plating with an arc vaporization basis, and (h) ion beam-assisted deposition (IBAD) with a thermal evaporation basis and ion bombardment from an ion gun [60].

2.7 Plasma electrolytic oxidation (PEO) coating method

2.7.1 Development of PEO method

PEO technique utilizes electrochemical surface treatment to produce oxide coatings on substrate materials to develop the wear and corrosion behavior of the substrate surface. It is particularly suitable for the surface treatment for aluminum,

magnesium, titanium and their alloys. The coating products are widely used in construction, transportation and automotive industry. It developed from conventional anodic oxidation and gradually forms different advanced coating techniques.

A summarized timeline for the development of micro-arc oxidation (MAO) is illustrated in Figure 2.13. A.L. Yerokhin et al. had a review on the history of PEO coating. The electrolytic spark discharge phenomenon was found in the 1880s. Gradually in 1930s the detailed study of discharge effects in electrolytes were studied. The 1960s saw the practical example of cadmium niobate coating on cadmium substrate. The PEO coatings are widely used on aluminum alloys in 1970s and a variety of patents are made since then. For the coatings on light metals, the Russian workers made efforts on them. In the past 10 years, PEO coating with high quality, high thickness and durability are demanded. And light weight alloys with high strength are becoming the main substrate material [61].
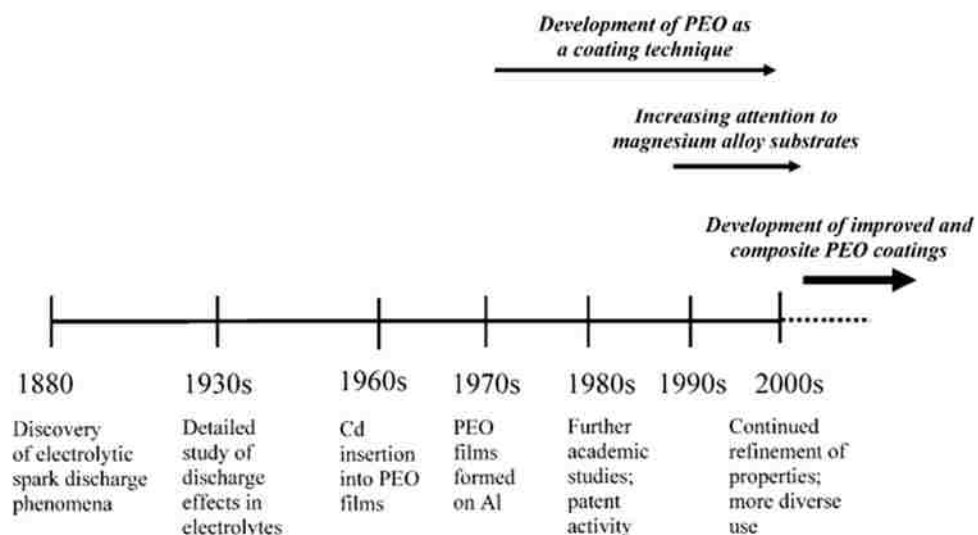
Figure 2.13 Basic time line illustrating development of PEO coatings [61].

2.7.2 PEO coating process

All metal sheet and ingot are cut into small samples with specific size. The pieces are polished before used as the substrate materials for coatings. The irregular spurs will be eliminated by grinding machine. And the samples will be degreased in acetone solution in room temperature. After the preparation before coating, the sample will connect to the anode of the power equipment and be put into the reaction bath. The cathode of power equipment is connected with a counter electrode. The PEO reaction solution and parameters will be adjusted according to substrate material.

The coating deposition equipment is transferred from the anodizing process. Figure 2.14 show schematic PEO deposition machine [59] .The processing equipment includes two parts: power supply and reaction bath (Figure.2.14 (b)).The reaction bath has a water-cooler system to prevent high operation temperature. It is connected with a dielectric base and covered by a plastic cover. It's easy to observe the reaction from outside the electrolyte bath. The metal sample is immersed into the electrolyte and is regarded as the working electrode. The counter electrode utilizes the stainless steel plate that is linked with base [62-66].

There are multiple power sources that are used for coating process. According to the current type the power source can be classified as: DC sources, unbalanced AC sources, pulsed DC sources and heteropolar pulsed current sources [65]. In this study, two pulsed DC power source is used to deposit films on the three substrate materials. Two pulsed DC power supply are united with working electrode and counter electrode. Under this power operation, the different current waveforms will be obtained. In the coating process, the voltage increases gradually with treatment time. For different metal samples, the unipolar current modes and bipolar current modes are used respectively.
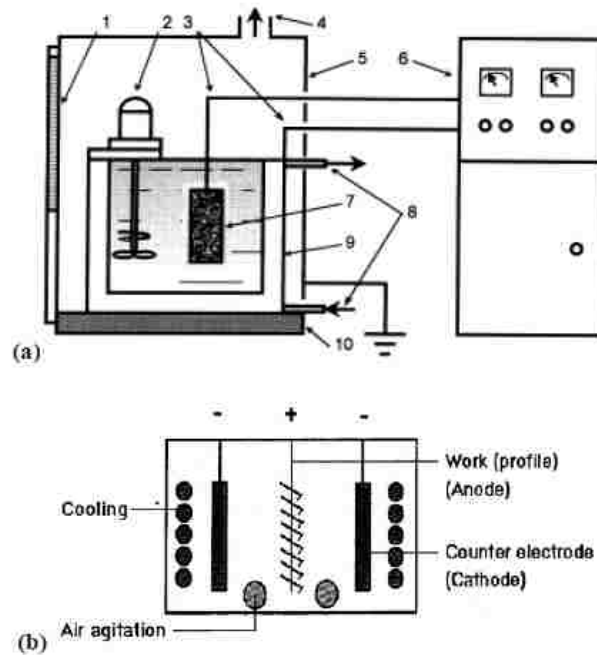
Figure 2.14 (a) Typical treatment part for PEO process: 1. window, 2. mixer, 3. linking wires, 4. exhaust/ventilation system, 5. grounded cover, 6. power supply component, 7. work sample, 8. cooling system, 9. reaction bath, 10. insulating plant. (b) Electrolyte bath [61].

2.7.3 Current-voltage characteristics of PEO process

During plasma electrolysis process, the current-voltage diagrams are given in figure 2.15. Yerokhin et al. [59] summarize current-voltage trend for plasma electrolysis. The "type-a" current-voltage plot shows a metal-electrolyte system with basic gas liberation on either the cathode or anode surface; "type –b" describes the current-voltage plot when oxide film formation happens. The current increases proportionally with the increase of voltage in the region "0-U_1" of type-a system and region "0-U_4" of type-b system. Nevertheless, the current trend becomes complex with the change of voltage.

In the type-a system, the increase of potential causes current oscillation with the phenomena of luminescence. The current goes up until a limited value since gaseous reaction products (O_2 or H_2) will appear on the electrode surface and form a shield. The reaction between remaining exposed electrode and electrolyte will lead to electrolyte boiling near the electrode. The electrode is covered by gaseous vapour plasma in the electrolysis process that approaches to U_2, which inhibits the electrical conductivity of electrode. The electric field strength E near the electrode will increase significantly due to the concentration of voltage in the near-electrode region. Accompanied with the E increase, a rapid sparking appears in scattered gaseous bubbles and then becomes a unique glow throughout the covered electrode. The cover on the electrode makes a drop on current in the region U_2-U_3 while the current increase of current beyond U_3 is caused by the transformation from glow discharge to intensive arcing.
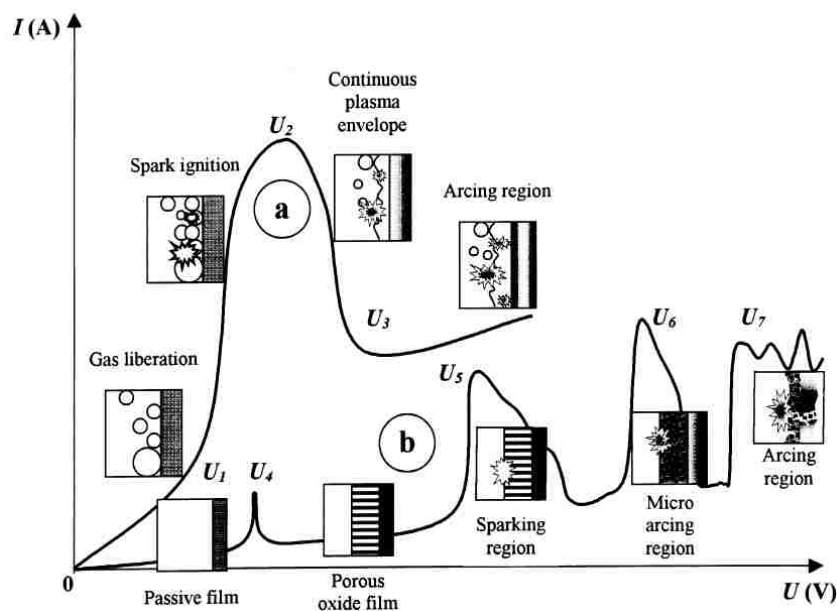
Figure 2.15 Two kinds of current-voltage figure for the processes of plasma electrolysis: discharge phenomena are established (a) in the near-electrode zone and (b) in the dielectric film on the electrode surface [61].

The type-b system is a little bit complicated. The passive film forms in the region from U_1 to U_4. A porous oxide film appears in the region U_4-U_5 because of repassivation. The electric field strength decreases after U5 since the film breaks under impact. The sparking will happen during the section of U_5-U_6. At point U6, thermal ionisation begins and will be blocked by the discharge decline of substrate. Since the thickness of the film increases with time and it will shield the substrate gradually. This micro-discharges caused by discharge decline is somehow called "micro arcs". And this process contributes to the formation of thin film in the electrolyte. Beyond point U_7, the discharge decline no longer exits and these micro charges will cause thermal cracking of the film.

2.7.4 Electrolyte selection for PEO

PEO electrolyte is really important in the electrolysis process. According to the films formed on aluminum, there are six groups of electrolyte selection which is shown in figure 2.16. They can be classified:

1. Solutions that boost dissolution of aluminum, e.g. $NaClO_3$, $NaCl$;

2. Solutions that decrease dissolution of metal, e.g. Na_2SO_4, H_2SO_4;

3. Electrolytes that offer passivation of metal, e.g. phosphoric acid and sodium acetate.

4. Electrolytes that have complex effects such as KF and NaF;

5. Solutions that provide slight passivation;

6. Solutions that offer obvious metal passivation, e.g. inorganic polymers, boric acids, phosphoric acids and salts of carbonic.
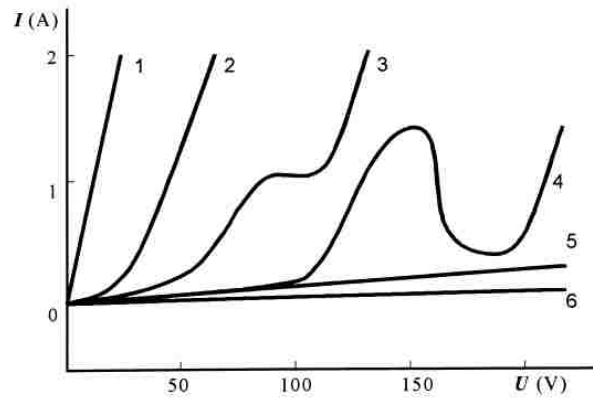
Figure 2.16 The function I=f (U) of several electrolytes confirmed for PEO treatment of aluminum. Anodic polarization can cause: (1) quick metal dissolution, (2) slow metal dissolution, (3) metal passivation in slight voltage interval, (4) multifaceted behaviour with a wide break of passivation, (5) slender passivation and (6) strong passivation of the metal [68].

2.7.5 PEO coatings on aluminized steel

PEO process is a breakthrough for the traditional technique of anodic oxidation. PEO coating often has high insulation resistance, good corrosion resistance, good wear resistance and high micro hardness. Due to those unique properties, PEO coating applications appear a lot in mechanical and electrical industry in recent years. About the coating above the aluminized steel, several researchers have given a solid foundation. The thickness change, element composition and layer distribution were analyzed for coatings on aluminized steel. And this thesis paper focus more on the corrosion resistance of PEO coatings on aluminized steel. Also the surface morphology is analyzed in this thesis paper.

Table 2.2 Summary of research about PEO coatings on aluminized steel.

researcher	substrate	PEO electrolyte	PEO power	Focus
Wenbin Xue et al.[68]	Al-Cu-Mg alloy	5g/L NaOH	AC	Thickness of coating
Shengxue Yu et al. [69]	A3 steel with aluminum layer	10g/L Na_2SiO_3 and 2g/L NaOH	AC	Coating element distribution of composite coating
Zhongshi Yang et al. [70]	Hot dip aluminized steel	5g/L NaOH and 30g/L Na_2SiO_3	AC	Coating element distribution
Weichao Gu et al. [71]	Q235 steel with aluminum layer	5% NaOH and other additives	-	Surface morphology
Weichao Gu et al. [72]	0.20 wt.% C steel with aluminum layer	NaOH, Na2SiO3 and NaPO3	-	Coating layer determination

The coating performance is summarized in table 2.2. The substrate materials are all aluminized steels or aluminum alloys. The aluminum oxide films above steel are always made by hot dip method. PEO is carried out with different solution plans. Weichao Gu et al. [71] examined the duplex coating surface by scanning electron microscopy (SEM) and X-ray diffractometer (XRD). It is found that the outer ceramic coatings include α-Al_2O_3, γ-Al2O3 and θ-Al2O3. The duplex coatings have better corrosion and wear resistances. And this combination of PEO and arc spraying offer the steel substrate a hopeful way to prevent corrosion and friction. The SEM micrographs of the coating surface for different treatment time are shown in figure 2.17.
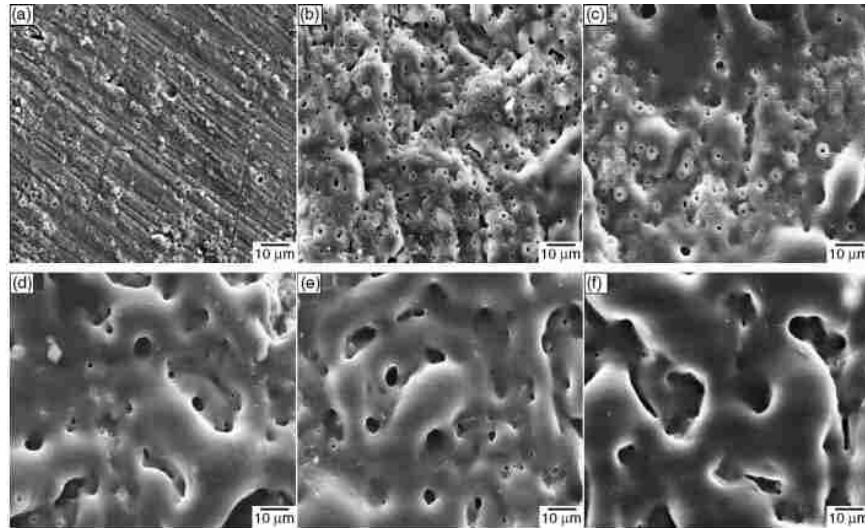
Figure 2.17 SEM micrographs of the coatings surface with different time for (a) 45 s, (b) 10min, (c) 25min, and (f) 35min [71].

Weichao Gu et al. [72] found that hot-dip treatment will add two layers (Al and $Fe_xAl_{(1-x)}$) to the steel substrate. And PEO coating is the uniform Al_2O_3 ceramic coatings. The main compositions of ceramic coating are α-Al2O3 and γ-Al2O3.The ceramic coating can prevent corrosion. The cross-section picture and corresponding EDX results of PEO coating and hot-dip film are described respectively in figure 2.18 and figure 2.19.
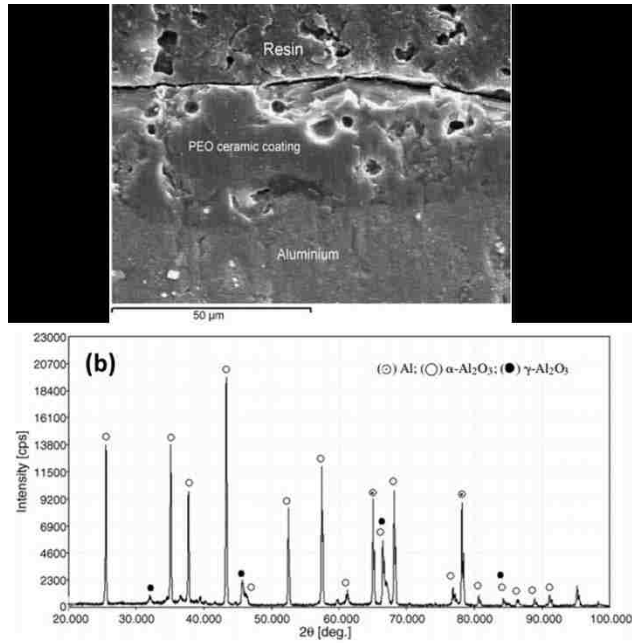
Figure 2.18 SEM image of cross-section zone in coated aluminum and EDX analysis of PEO ceramic coating [72].
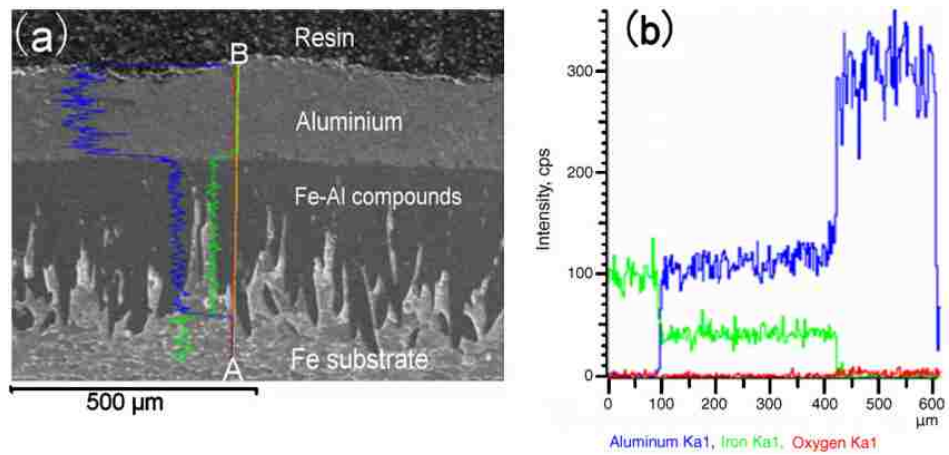
Figure 2.19 SEM image of cross-section zone in aluminized steel and EDX analysis of the hot-dipping coating [72].

2.7.6 PEO coating on magnesium alloys

Magnesium is one of the most promising lightweight materials and is used in many future applications. However, it is important to coat the substrate magnesium due to limitations of their inferior corrosion resistance and poor wear resistance. In recent years, the coating surface morphology, corrosion resistance and wear resistance are the vital parts in research papers. The effects of pulse timing, electrolyte, substrate material and current mode on PEO coating properties are studied by R.O. Hussein et al.. Table 2.3 below shows recent results about the ceramic coatings on magnesium.

Table 2.3 Summary of coatings on magnesium alloys.

Researcher	Magnesium alloy	PEO electrolyte	Focus
Y. Ma et al. [73]	Pure magnesium	Na_2SiO_3 or Na_2PO_4, and KOH	Electrolyte effect on corrosion resistance
R.O. Hussein et al. [74]	AM60B	$K_4P_2O_7$, $Na_2Al_2O_4$ and KOH	The effect of pulse timing and current mode on corrosion resistance
R.O. Hussein et al. [75]	AJ62	$Na_2Al_2O_4$ and KOH	Coating growth mechanism
R.O. Hussein et al. [76]	AM60B AJ62 AZ91D	$Na_2Al_2O_4$ and KOH	Influence of processing parameters and substrate composition on corrosion resistance
R.O. Hussein et al. [77]	AM60B	$K_4P_2O_7$, $Na_2Al_2O_4$ and KOH	The effect of hybrid current modes on tribological properties

R.O. Hussein et al. [78] used different processing parameters for PEO coatings on different substrate magnesium alloys in PEO process. They get conclusions from factors like current modes, treatment time and substrate magnesium selections. The results show that alloying elements and oxidation treatment time are key factors that have significant influences on surface morphologies, porosity level and coating thickness. And as the treatment time increases, corrosion performance becomes good due to less porous surface situation. The ranking for corrosion resistance in potentiodynamic polarization test is: coated AZ91D> coated AM60B> coated AJ62 > coated pure Mg > uncoated Mg. In addition, R.O. Hussein [77] found that bipolar current mode could help improve tribological performance in both inclined impact-sliding test and pin-on-disc test. The SEM micrographs of surface morphology and cross-sections of coatings are shown in figure 2.20 and figure 2.21 respectively.
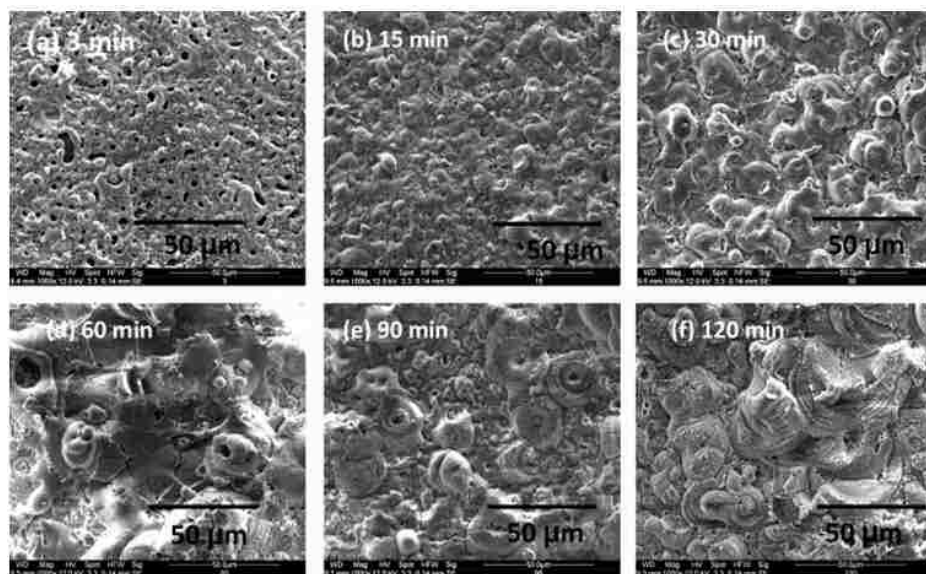
Figure 2.20   SEM micrographs showing the surface morphology of PEO coatings above AJ62 for different processed times [75].
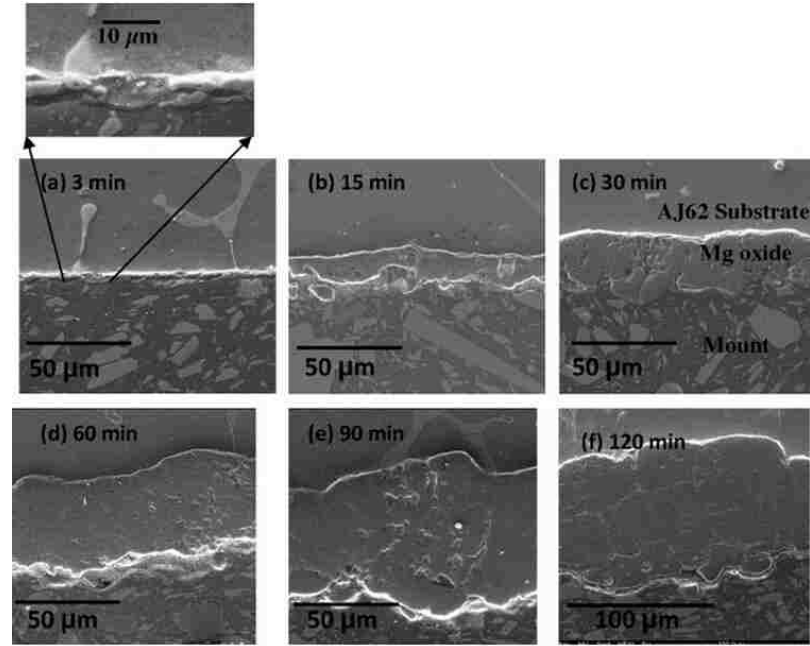
Figure 2.21 SEM micrographs of cross-section zone of coatings deposited on AJ62 for different treatment times [75].

Figure 2.22 shows the potentiodynamic polarization curves of uncoated AJ62 Mg alloy and coated samples (different current modes). The corrosion resistances of all the samples are calculated due to current density and tafel slopes that are derived from the figure. The table summarize important values in the curve and final corrosion resistances of all the samples.

Table 2.4 Effect of current mode and alloy composition on the corrosion protection efficiency of PEO-coated Mg-alloys [74].

	Mg alloy	Uncoated	Unipolar	Bipolar	Hybrid
E_{corr} (V)	AM60B	−1.511	−1.46	−1.43	−1.48
	AJ62	−1.58	−1.54	−1.42	N/A
I_{corr} ($\mu A/cm^2$)	AM60B	35.3	0.316	0.072	0.0071
	AJ62	22.4	0.54	0.012	N/A
R_p ($\Omega\ cm^2$)	AM60B	2.76E+02	5.84E+04	8.35E+05	4.54E+06
	AJ62	7.11E+02	4.10E+04	1.24E+06	N/A
$P_{EF}\%$	AM60B	–	209	3015	16450
	AJ62	–	56.6	1743	N/A
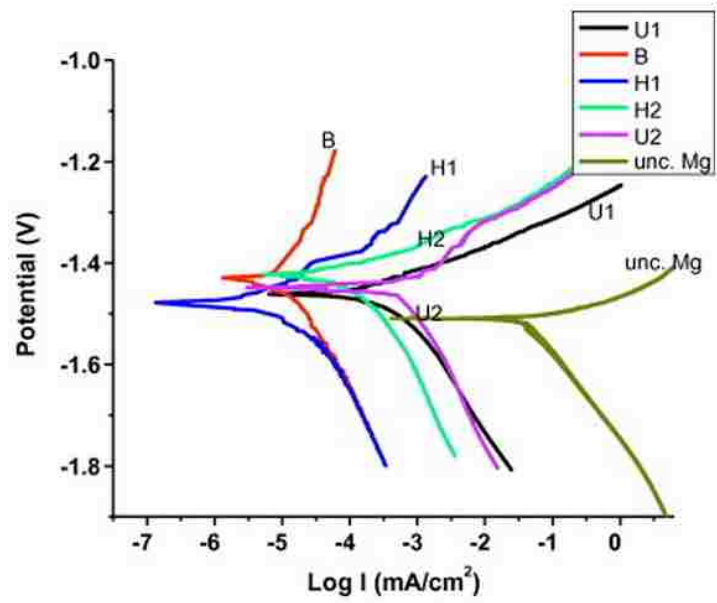
Figure 2.22 Potentiodynamic polarization curves showing the uncoated (unc.Mg) and coated samples with unipolar (U1 and U2), bipolar (B) and Hybrid (H1 and H2) current modes [74].

Chapter 3: EXPERIMENTAL PROCEDURES

In this chapter, the trial techniques used for the coating of the PEO ceramic coatings on substrate materials (aluminized steel, aluminized AHSS and magnesium) and the study of their corrosion properties are illustrated. PEO method was employed for coating preparations on those substrates. In particular, two current modes (unipolar and bipolar) were applied to coat magnesium. The corrosion resistance was determined by potentiodynamic polarization test. Surface morphology and cross sectional structures of coatings were characterized by scanning electron microscopy (SEM). The coating prospects of aluminized steel, aluminized AHSS and magnesium in galvanic couples were investigated by ZRA corrosion tests. The roles of PEO coatings on the steel and Mg samples in corrosion behaviors of the alloys and their couplings were analyzed in the following sections.

3.1 Sample preparation

Aluminized steel sheet (3 millimeters in thickness) was cut into square pieces with the length of 30 millimeters. A number of the square samples were heated in a furnace to 400°C or 900°C for 10 minutes. The heated samples were then placed on a large steel plate for fast cooling in air. The treated samples, called aluminized AHSS, were divided into two groups by temperature (400°C and 900°C) for coating preparations and corrosion tests. It should be noticed that the treated steel might not become a real AHSS due to either low treatment temperature (400°C) or inefficient cooling rate, but the Al surface layer had experienced a heating/cooling process similar to hot stamping operation. The status of sample surface was of main concerns in this study.

A magnesium ingot (AZ35) was cut into square pieces with a dimension of 25 millimeters long, 25 millimeters wide and 8 millimeters high. The pieces were polished before used as the substrate materials for coatings. The irregular spurs along the cut edges of square pieces were eliminated by an abrasive grinding machine. The samples were degreased in acetone before dried in an ambient condition. The substrate material of magnesium and aluminized steel are shown in figure 3.1
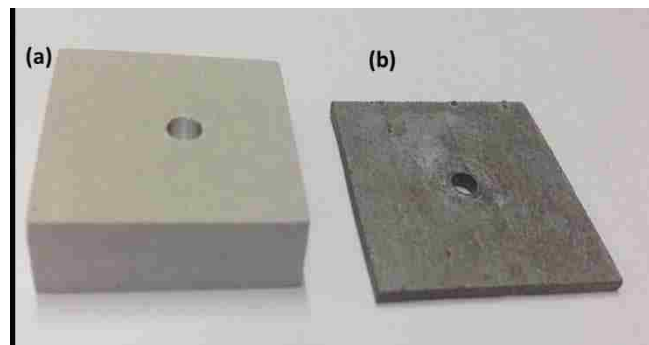
Figure 3.1 Magnesium substrate sample (a) and aluminized steel sample (b).

3.2 Deposition process for PEO coatings**.**

A PEO coating method was used to prepare oxide coatings on aluminized steels. During the PEO process treatment, aluminized samples were connected to the positive output of a power supply and a stainless steel plate to the negative output. For preparation of an electrolyte, 50-100 g potassium-titanium oxalate, 5-13 g citric acid, 5-15g potassium hydroxide and other additives were dissolved in 3 liters of distilled water (solution plan 1). The pH of the solution was around 7. The treatment time was 1min, 2min, 3min and 4min respectively. The aluminum layer on the aluminized steel was oxidized to an aluminum oxide incorporated with oxide from the electrolyte solution during the plasma electrochemical oxidation process. In the coating process, there are five electrolyte plans. Solution plan 2 includes Na_2SiO_3 and KOH. The other electrolyte solution plans are designed with weight ratio (plan1/plan2) of 1, 0.5

and 2 respectively. And they are named as plan 3, plan 4 and plan 5 respectively according to the electrolyte ratio.

Aluminized AHSS were obtained by thermal treatment at 400℃ and 900℃ respectively. Then, repeat same coating method on aluminized AHSS to obtain a PEO coating.

The coating on magnesium was obtained in an alkaline electrolyte containing sodium aluminate (2-6 g/l Na2Al2O3) and sodium phosphate (2-6 g/l Na3PO4) with different treatment time and current modes. The temperature of the electrolytes was kept below 25 °C by a water cooling system.

During the coating process, the voltage was increased gradually with process time to maintain a constant current while the coating thickness was increased. To examine the effects of current mode on the resultant properties of the coatings, the PEO coating process was carried out using two different current modes: unipolar and bipolar current modes. Process parameters, such as the frequency (f=1/T, where T is the pulse period), the duration of each pulse (Ton + and Ton −, the period of positive and negative pulse respectively) and the resting gap (break) between the positive and negative pulses (Toff + and Toff − respectively) are listed in table 3.1.

Table 3.1 PEO process parameters for coating depositions on Mg.

sample	PEO Treatment time	Current mode	I^+ (A)	I^- (A)	T^+on us	T^+off Us	T^-on us	T^+off Us
Mg		unipolar	1.23		400	100		
U6	6min	unipolar	1.23		400	100		
U12	12min	unipolar	1.23		400	100		
U18	18min	unipolar	1.23		400	100		
B6	6min	bipolar	1.23	1.07	400	100	400	100
B12	12min	bipolar	1.23	1.07	400	100	400	100
B18	18min	bipolar	1.23	1.07	400	100	400	100

3.3 Corrosion test

3.3.1 Potentiodynamic polarization test

A three electrode corrosion test method (figure 3.2) was used to polarize the testing sample. The current vs. potential response was measured as the potential was shifted away from the corrosion potential at open circuit (0.2mV/s). The test was operated in a NaCl solution with 3.5% mass percentage. The polarization resistances were calculated from the examination results. The contact area of the samples exposed to the corrosive condition was 1 cm^2. The ratio of the volume of NaCl solution/sample area was 300ml/cm2. After the electrochemical testing system became stable (20 to 30min), scans were conducted at a rate of 1mV/s from -0.5V versus open circuit potential in a more noble direction up to +2V versus the reference electrode.
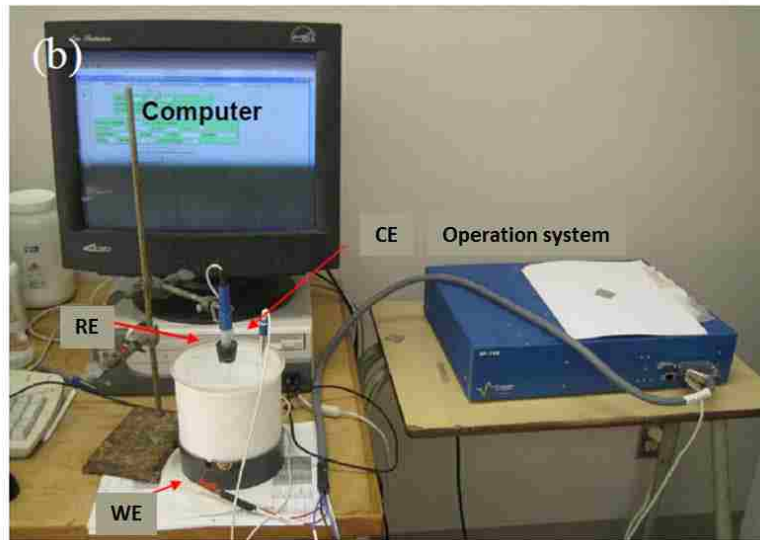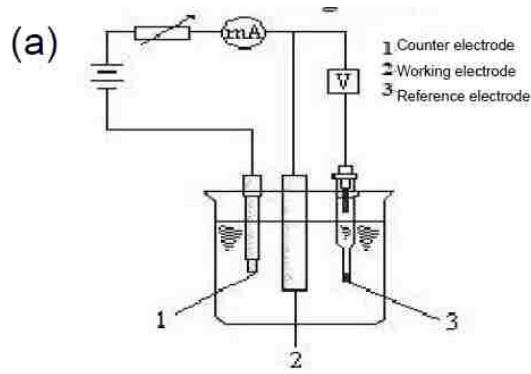
Figure 3.2 (a) Three-electrode cell and (b) Electrochemical polarization corrosion testing equipment [67].

The determination of corrosion current density by extrapolation of linear parts of the polarization curves is illustrated in figure 3.3. The region of linearity is referred to as the Tafel region. The intersection point between the extrapolated Tafel regions gives the corrosion current density (icorr). The corrosion resistance is calculated by the equation below by using three important values derived in the figure 3.3

$$\mathrm{Rp} = \frac{\beta a \times \beta c}{2.3 \, Icorr(\beta a + \beta c)}$$

Where βa and βc are the Tafel slops of the anodic and cathodic reactions respectively. The term corrosion resistance Rp ($\Delta E/\Delta iapp$) is given in ohms (volts/amperes or millivolts/milliamperes). If the beta values for the reaction are known, corrosion rate may be calculated by this equation.
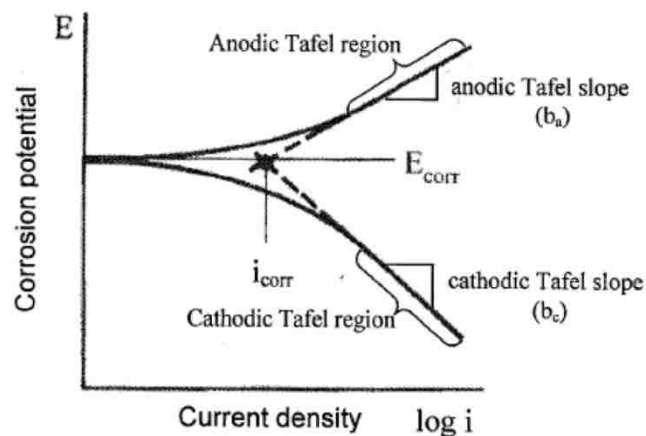
Figure 3.3 Determination of corrosion current density and corrosion potential by extrapolation of linear zone of the polarization curve [78], icorr—corrosion current density, Ecorr—corrosion potential.

3.3.2 Zero resistance ammeter (ZRA) corrosion test

The test samples were immersed in 3.5% sodium chloride water at room temperature. Before the corrosion tests, each specimen was held at its rest potential for about 15min to reach a stable corrosion potential. The steel samples including steel, aluminized steel, PEO-coated aluminized steel, aluminized AHSS, and PEO-coated aluminized AHSS, were used as the cathode in the corrosion cell. Magnesium or PEO-coated magnesium was used as the anode. The potential difference between the cathodic and anodic samples is the driving force of corrosion in this experiment. The galvanic current density was recorded as a function of time (4 hours). The exposure area ratio (specimen of anode versus cathode) was 1:8 for each testing

combination. The schematic view of the three electrode cell of ZRA test is described in figure 3.4.
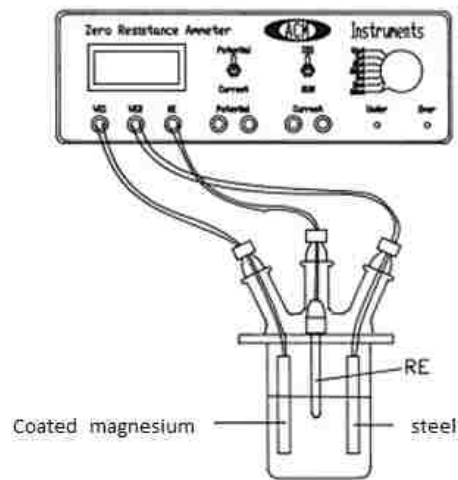
Figure 3.4 Zero resistance ammeter (ZRA) corrosion test [79].

3.3.3 Boiling test

As mentioned in the ZRA test, the galvanic corrosion performance among galvanic couples are tested by the ZRA test and boiling test. There are four couplings that are between steel samples and magnesium samples. The steel samples including aluminized steel, PEO-coated aluminized steel, aluminized AHSS, and PEO-coated aluminized AHSS, were used as the cathode in the corrosion cell. Magnesium or PEO-coated magnesium was used as the anode. The potential difference between the cathodic and anodic samples is the driving force of corrosion in this experiment. And boiling test utilizes same galvanic couples as in the ZRA test. Two samples are connected by plastic bolts and nuts. The connected boiling sample is put in the 3.5% sodium chloride solution. The boiling treatment time is one hour and heating temperature is 100 ℃. After boiling test, the SEM method and polarization corrosion test are used to analyze the after-boiling surface. The following images show the boiling test equipment (figure 3.5(a)) and boiling samples (figure 3.(b)) respectively.
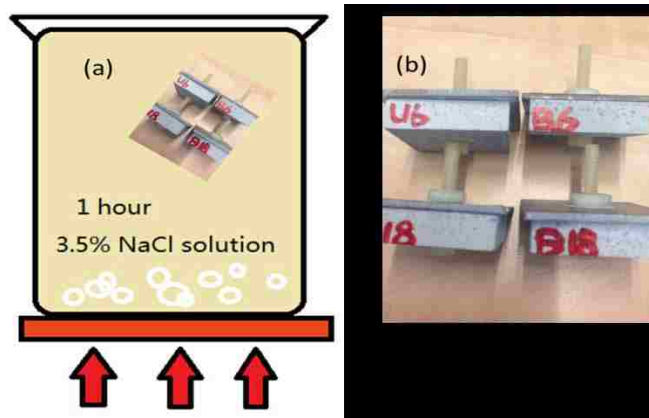
Figure 3.5 (a) Boiling test equipment (b) Boiling test samples.

3.4 Scanning electron microscope (SEM) analysis and energy dispersive spectroscopy (EDS).

A scanning electron microscope with energy dispersive X-ray analysis (EDX) was utilized to observe the sample surface morphologies and cross-sections. The FEI Quanta 200 FEG microscope (Figure 3.6) was purchased in 2005, and is a leader in high resolution SEM with the following equipment and provisions: field emission gun (filament) for highest resolution scanning electron microscope and workstation; everhart-thornley secondary electron detector; solid state backscatter detector; large field secondary electron detector; EDAX energy dispersive spectroscopy (EDS) X-Ray detector; gaseous secondary electron detector [77]. The 3-mm-thick aluminized steel samples were mounted with resin and polished to a mirror finish. Chemical compositions of selected samples were analyzed by the EDS method (shown in figure 3.6).

47

Figure 3.6 The FEI quanta 200 EFG microscope in Great Lakes Institute [80].
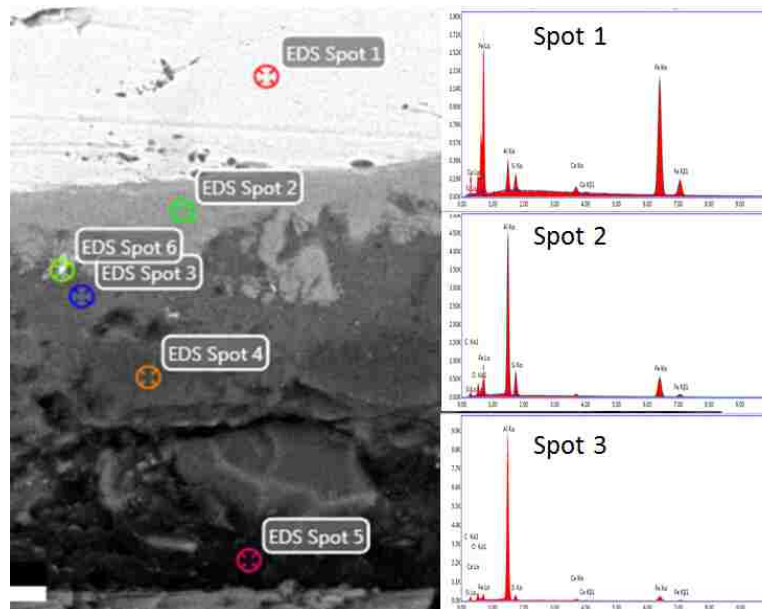
Figure 3.7 Screen image of the EDAX energy dispersive spectroscopy interface showing the element analysis of cross-section in coating layer above aluminized steel.

Energy Dispersive Spectroscopy (EDS), also known as X-Ray Analysis, is a very powerful tool on SEM which allows you to identify the elements present in your sample. A very small spot or a whole frame can be analyzed for the elemental composition of the sample with high accuracy and resolution. The EDS can run from the Secondary Electron Image, or the Backscatter Image, and works using any mode

of the microscope (High Vacuum, Low Vacuum, and Environmental Mode). This is a valuable instrument for many fields of research containing engineering, chemistry, geology and biology. The technique is non-destructive, fast and user-friendly. EDS can be operated standard less, or with pre-determined standards, and delivers qualitative and quantitative data about the elemental composition of the sample [80].

3.5 Surface roughness measurement

The surface roughness of coatings on aluminized steel samples is detected by the mitutoyo SJ-201P surface profiler (Figure 3.8) with a data-summarize system.
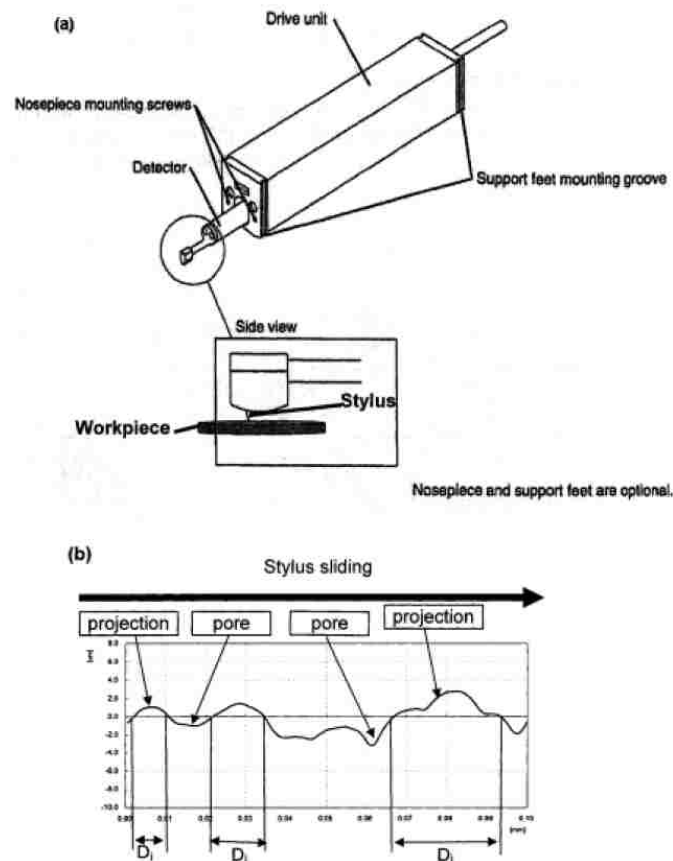
Figure 3.8 Equipment for surface roughness of coating: (a) the detector component of surface profilometer and (b) a characteristic surface profile plot [67].

3.6 Pin-on-disc tribology test.

The tribology test is used on the coating surface of aluminized steel. This Sciland Pin/Disc tribometer PCD-300 a (figure 3.9) is operated in ambient temperature. There are two operation mode: rotating mode (sliding speed: 0.05 m/s) for flat samples and reciprocating mode (sliding speed: 0.08m/s) for the curved samples. In this study, only the rotating mode is used for the flat coating surface of aluminized steel. The test was carried out using a steel ball pin (SAE 51200 steel) as the counter face material in the ambient condition under a 1 N load for 200 m sliding distance. The diameter of the circle of the wear track was 4 mm and the sliding speed was 0.05 m/s. The ball was fixed and the sample was rotated to obtain the wear track. The coefficient of friction was recorded with the increase of the sliding distance.
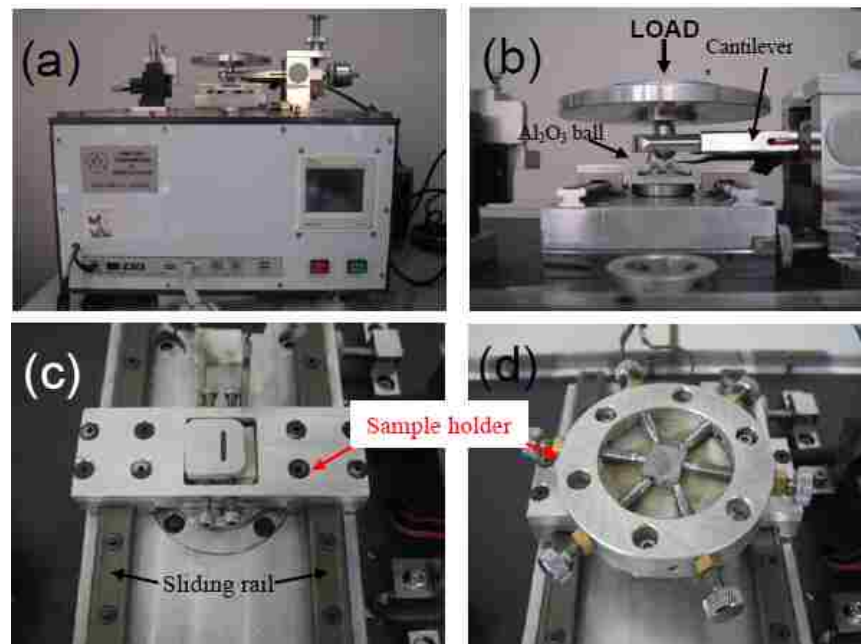
Figure 3.9 Sliding tester attached on (a) Sciland Pin/Disc Tribometer PCD-300A (b) load component and cantilever beam, (c) working piece holder for reciprocating mode (d) working piece holder for rotating mode [67].

3.7 Thermal transfer test

The uncoated sample and 3-min coated sample are respectively fixed above a stove and placed between two thermometers. The samples were 3 mm and 50 mm away from the thermometers and stove respectively. The temperatures of four locations (stove, lower thermometer, upper thermometer and sample) were recorded every minute in a process of 20 minutes.
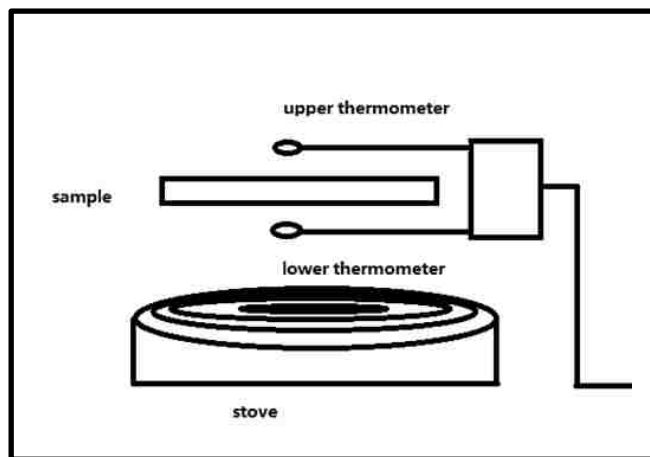
Figure 3.10 Setup illustration of thermal transfer test.

Chapter 4: EXPERIMENTAL RESULTS AND DISCUSSION

4.1 PEO coatings on aluminized steel

PEO coating is deposited on the aluminized steel for treatment time of 1min, 2min, 3min and 4min according to solution plan 1 respectively. The general corrosion behaviors of coatings with different treatment time are analyzed by polarization corrosion test (4.1.3). The comparison between 3-min coated aluminized steel and aluminized steel is studied by the Pin-on-disc test (4.1.1~4.1.2) and heat transfer test (4.1.3). The choice for 3-min coated sample in this comparison is due to that 3-min coated sample has highest corrosion resistance and best general corrosion behavior. The corrosion behaviors of coatings with other coating solution plans are discussed in 4.1.5 briefly.

4.1.1 Wear behavior of PEO-coated aluminized steel and uncoated sample

As-prepared PEO coatings were tested by POD under a 1 N normal load for a 200 m sliding distance in an ambient condition. The coefficient of friction (COF) vs. sliding distances of uncoated aluminized steel, 1-min coated aluminized steel and 3-min coated aluminized steel are shown in figure 4.1. The COF value of coated sample with 3-minute treatment time (in a range of 0.2-0.5) is lower than the value of coated sample with 1-minute treatment time (in a range of 0.5-0.8) and uncoated sample (in a range of 05-0.8). The fluctuation of COF values in the curve of 3-min coated sample indicates change in the contact area. In the coated sample prepared with a longer treatment time, the coating layer may consist of two parts: titanium-aluminum oxide top layer and aluminum oxide intermediate layer. The COF of titanium oxide is lower than the alumina [81]. Due to this, the unstable curve with increasing value of COF was recorded for 3-min while the intermediate alumina layer was gradually involved

with the proceeding of the sliding wear test. The overlapping part of the curve of uncoated sample and 1-min coated sample indicates that 1-min coated sample had a thin oxide coating layer on the substrate owing to a shorter coating treatment time, which may explains the treatment time has a significant effect on the wear resistance.

According to the Figure 4.2 where the roughness of surface of coatings are recorded by Mitutoyo surface profiler SJ201p, the average roughness Ra of uncoated sample and coated sample are Ra= 2.40 and Ra=2.50 respectively. The surfaces of coating on both sample are not so smooth but similar. The surface roughness should not contribute the COF difference between two PEO-coated samples.
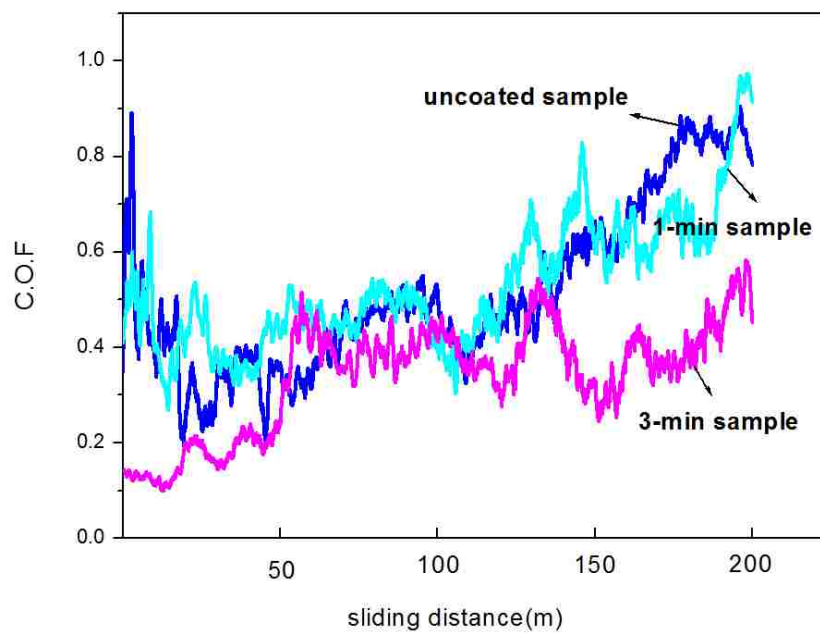
Figure 4.1 COF vs. sliding distance in POD wear tests at 1N load, 200m sliding distance for aluminized steel and coated aluminized steel (1-min sample and 3-min sample).
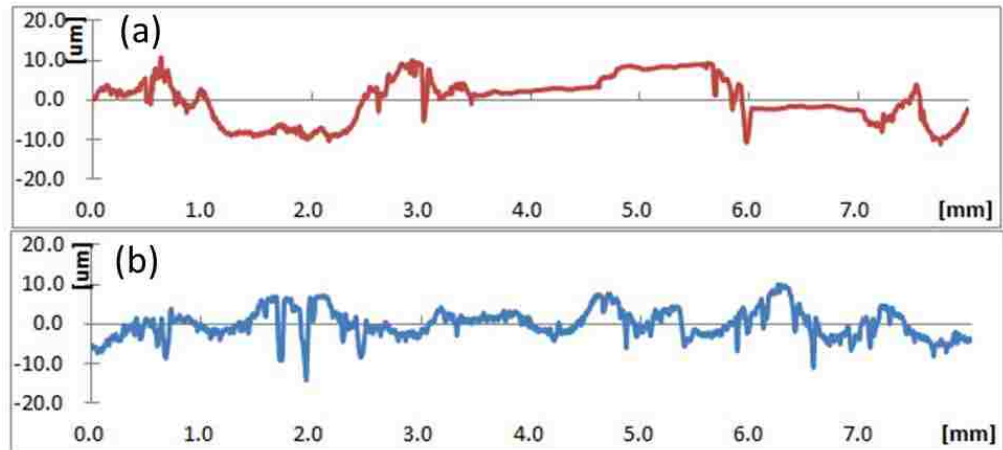
Figure 4.2 Surface roughness of samples: (a) uncoated aluminized steel and (b) 3-min coated aluminized steel are recorded by Mitutoyo surface profiler SJ201p.

4.1.2 OM Observations on POD wear tracks

The optical micrographs (OM) taken form wear tracks on the coatings are shown in figure 4.3. The 3-min coated aluminized steel has less damage than uncoated aluminized steel on the wear track of the circle after the POD tests. This indicates the PEO-coated sample has a better wear resistance. The wear track of a deeper and larger range of damage on the surface of the uncoated sample indicated partial elimination of the hot-dip aluminum layer. On the wear track of coated sample, the track was shallow owing to the coating wear protection provided from the titanium-aluminum oxide layer, on the steel, prepared by the PEO process.
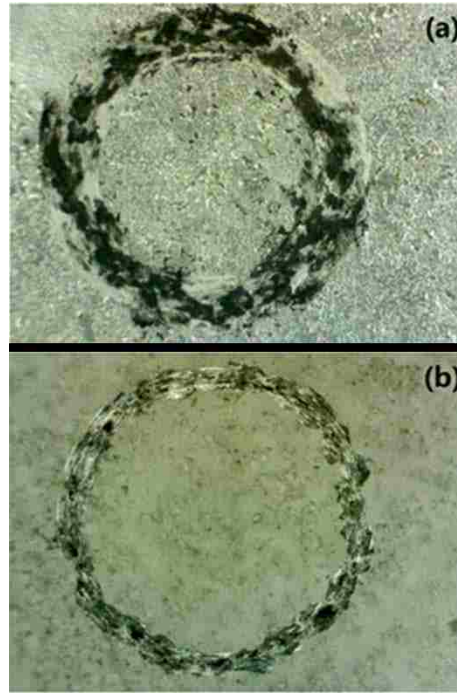
Figure 4.3 OM micrographs on POD wear tracks under 1N, 200 m condition. (a) uncoated sample, (b) 3-minute coated sample

4.1.3 Potentiodynamic polarization test

Aluminized steel samples were deposited with PEO coatings with different treatment time: 1min, 2min, 3min and 4min. The corrosion polarization curves of aluminized steel and those PEO-coated aluminized steel samples are plotted in Figure 1. Values of corrosion current density, Tafel slopes and corrosion potential are summarized in table 4.1, where it can be noted that the coated sample with 3 minute treatment time has the highest corrosion potential (-1.15 volts), the lowest corrosion current (3.16E-5 mA) and the highest corrosion resistance (R_p=260kΩ/cm^2). The polarization corrosion resistance R_p was calculated using the following formula [82]:

$$Rp = \frac{\beta a \times \beta c}{2.3 \, Icorr(\beta a + \beta c)} \, .$$

It can be seen from the graph that corrosion resistance increases when the samples were treated in the time range of 1 minute to 3 minutes. 4 min-coated sample does not follow this sequence and it has a relatively higher current (1.0 E-4 mA), lower potential (-1.3 volts) and lower resistance (1.03 E5 Ωcm^{-2}) comparing to the 3-min-coated sample. With the increase in treatment time, it is clearly noticed that porosity and pore size were significantly increased as shown in figure 4.4. The corrosion resistance of coatings on aluminized steel seemly depended on porosity of coating surfaces. The irregular and large pores as a result of 4-min treated sample suggest that the 4 minutes' treatment was too long, which could start to degrade the coating quality against corrosion. Even though, most of the coated samples behaved better than substrate aluminized steel. Hence, the PEO coating can be beneficial in effectively decreasing corrosion under certain corrosive conditions.

Table 4.1 Potentiodynamic polarization corrosion test results of coatings on aluminized steel in 3.5% NaCl solution.

	$E_{corr}(V)$	$I_{corr}(mA)$	$\beta a(mV)$	$\beta c(mV)$	$Rp(\Omega \cdot cm^{-2})$
Coated aluminized steel					
1min	-1.45	3.06 E-4	25.6	70.2	2.58 E 4
2min	-1.2	6.3 E-5	30.1	81.6	1.51 E 5
3min	-1.15	3.16 E-5	27.3	79.3	2.61 E 5
4min	-1.3	1.0 E-4	32.1	90.2	1.03 E5
Aluminized steel	-1.32	9.77 E-4	23.6	78.3	8070
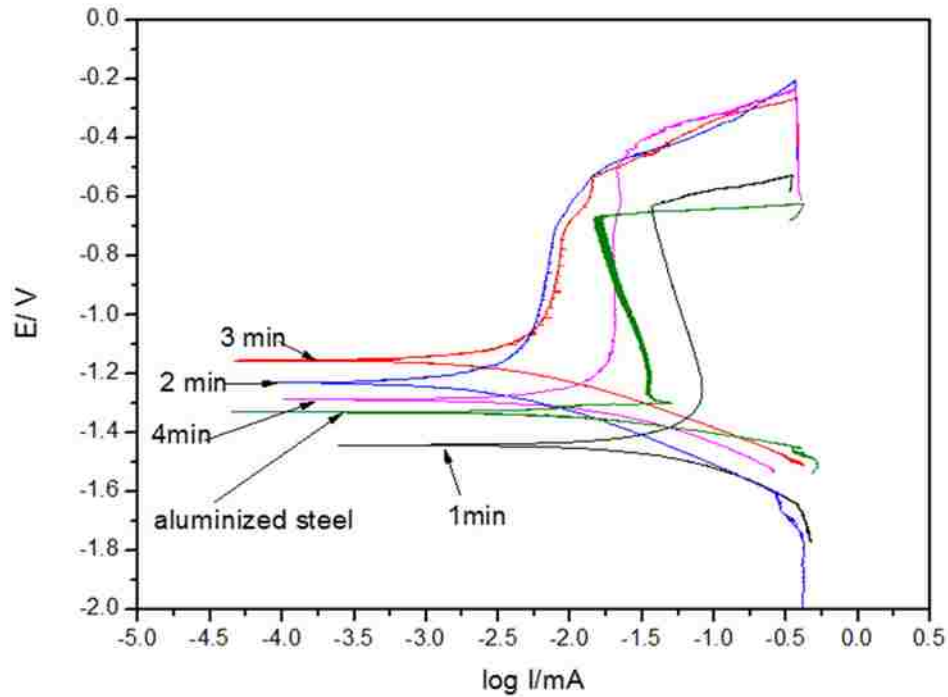
Figure 4.4 Polarization corrosion curves of aluminized steel and coated aluminized steel.

Comparison of the surface morphology of the coated and uncoated aluminized steel can be made through figure 4.5. Projections with micro-pores can be observed in all coated samples. In figure 4.5 (b), (c), (d) and (e), it can be found that the pores distribution was becoming wider. The coating sample with the longest treatment time had the largest pore sizes and widely distributed pores. During the PEO process, the molten alumina is generated due to the gas discharge in the channel from the substrate to the coating surface, which is abruptly ejected from the discharge channels to the top surface of the coating. Hence, various craters can be generated. With the treatment time further increasing, the surface of coating has more holes caused by the eruption of reaction product. The pores actually maintained small sizes and inconspicuous until
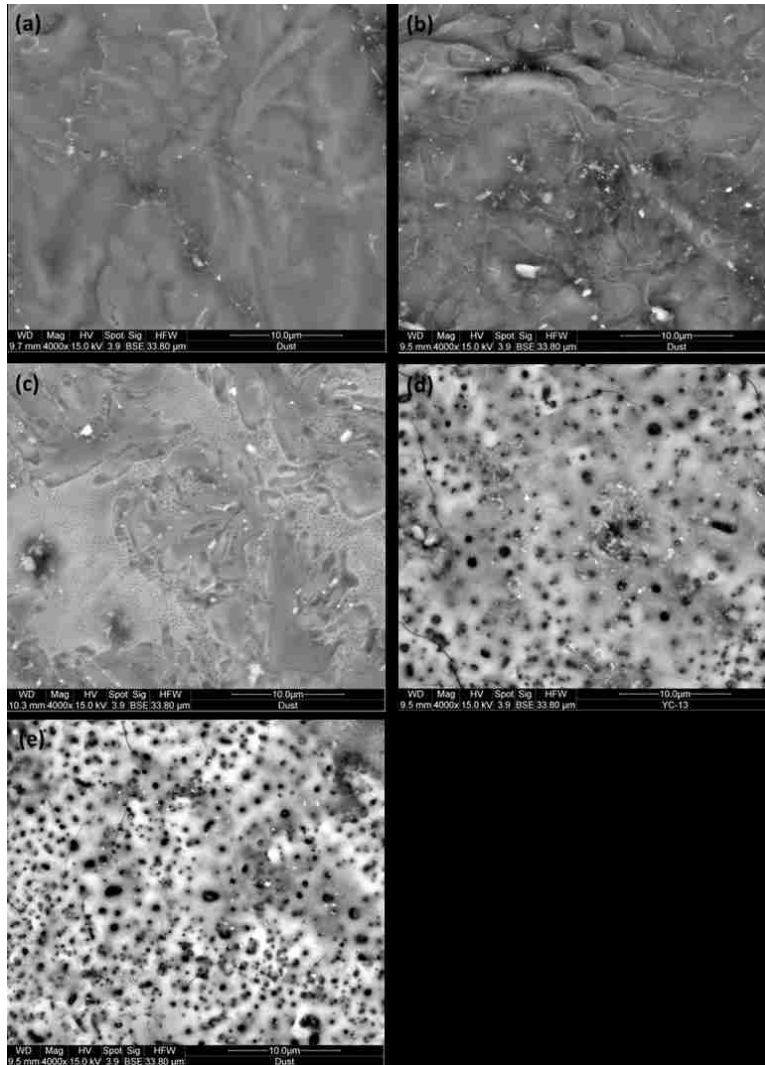
Figure 4.5 SEM micrographs using back-scattered electron mode showing the surface morphologies of coatings (a) uncoated, (b) 1min, (c) 2min, (d) 3min and (e) 4min.

the treatment time of coating growth was increased to 3 minutes. According to the above results of polarization corrosion test, coating with 3-min treatment time has the highest corrosion resistance. And this highest corrosion resistance could be owing to proper coating thickness and still small pores on the coating surface.

4.1.4 Thermal transfer test

Plots of temperature vs. heating time at different locations for cases of uncoated sample and 3-min coated sample are shown in figure 4.6 respectively. This test was

conducted in the ambient condition. The trends of stove temperature of both samples are nearly the same which confirmed the same heating-up process of the stove. The surface temperature of uncoated sample (in range of 170-180 ℃ when stable) is lower than that of coated sample with 3-min treatment time (in range of 200-205 ℃). The temperature of upper thermometer for the uncoated sample case (in range of 150-160 ℃) is lower than that of the 3-min coated sample case (in the range of 160-170 ℃). The temperature of lower thermometer of uncoated sample (in the range of 300-310 ℃) is nearly the same as 3-min coated sample (in the range of 300-310 ℃). These temperature differences indicate that the coated sample has better thermal absorption and emissivity properties.
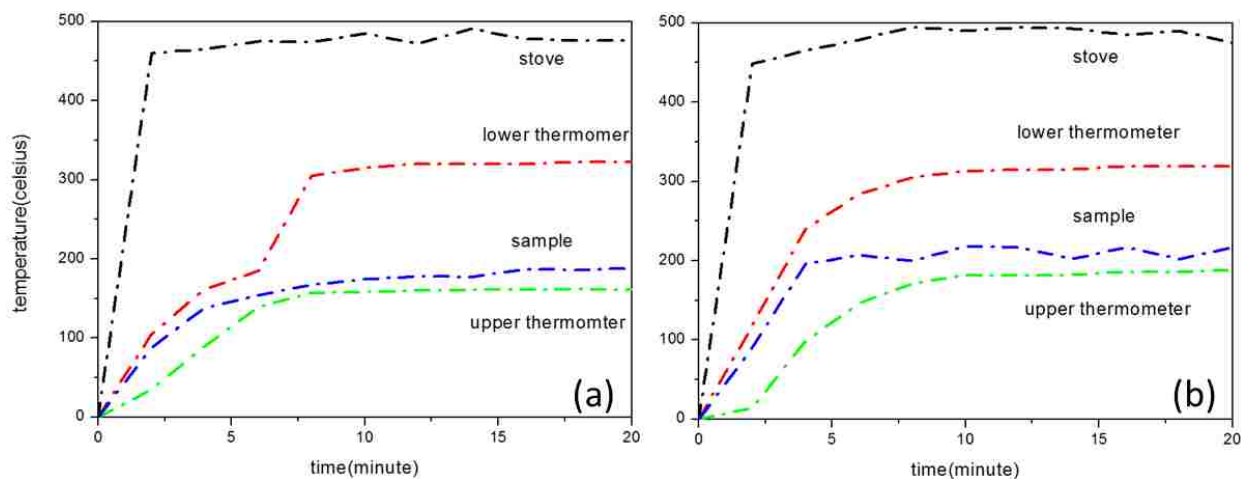
Figure 4.6 Temperature vs. heating time of different locations of samples: (a) uncoated aluminized steel and (b) coated aluminized steel with 3-min treatment time.

4.1.5 PEO coatings on aluminized steel using different electrolyte plan.

Figure 4.7 shows polarization corrosive curves of different solutions. For coating using S1 and S3, The best treatment time is 3 minutes. The coating (3min treatment time) shows best corrosive-resist behavior. Coating using S1 solution is being analyzed emphatically as discussed above.

59
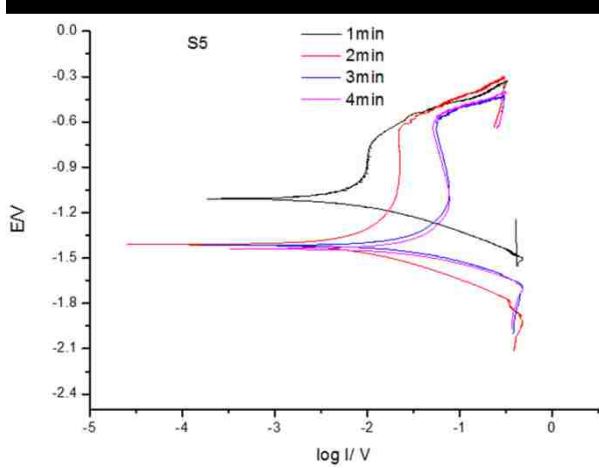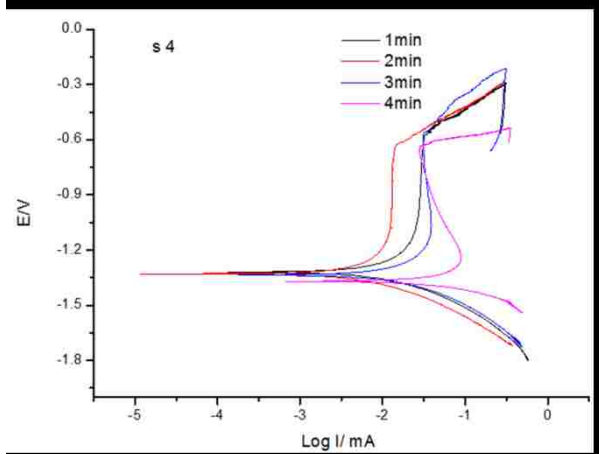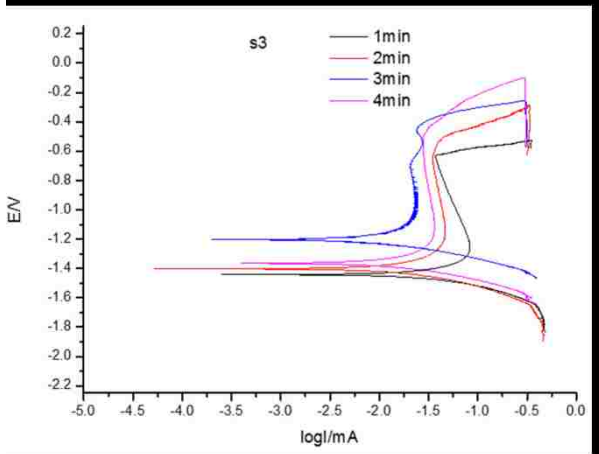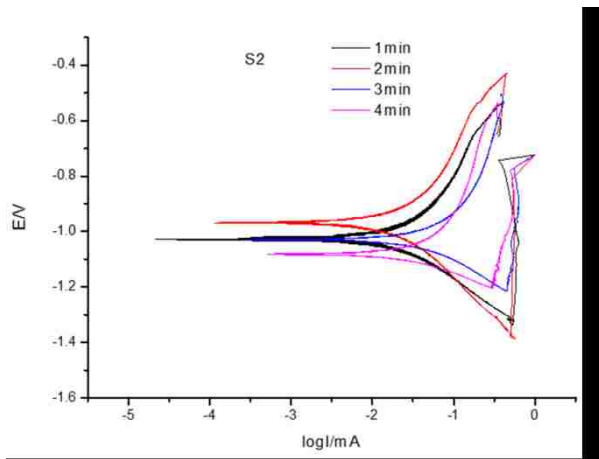
Figure 4.7 Corrosion curves of coatings using different coating electrolyte plan on aluminized steel

As we can see from the curves, aluminized steel has a higher corrosion resistance compared to steel. It verifies that an alumina layer can protect steel from corrosion, and that's and important reason why we choose aluminized steel as basic material in research. The corrosion resistance of coated samples is lower than that of steel. The coating corrodes first in galvanic corrosion so that it protects the substance material.

SEM picture of cross-section of coating (S1) and EDS analysis results are shown in figure 4.8 and figure 4.9 respectively. From Spot 1 to Spot 3, the content of element iron reduces and the content of element aluminum increases. That is the result of element penetration. It can be seen obviously that there exists steel, alumina and coating layer. However, the element titanium can't be found in the EDS analysis result. It maybe owes to the minimum value of titanium.
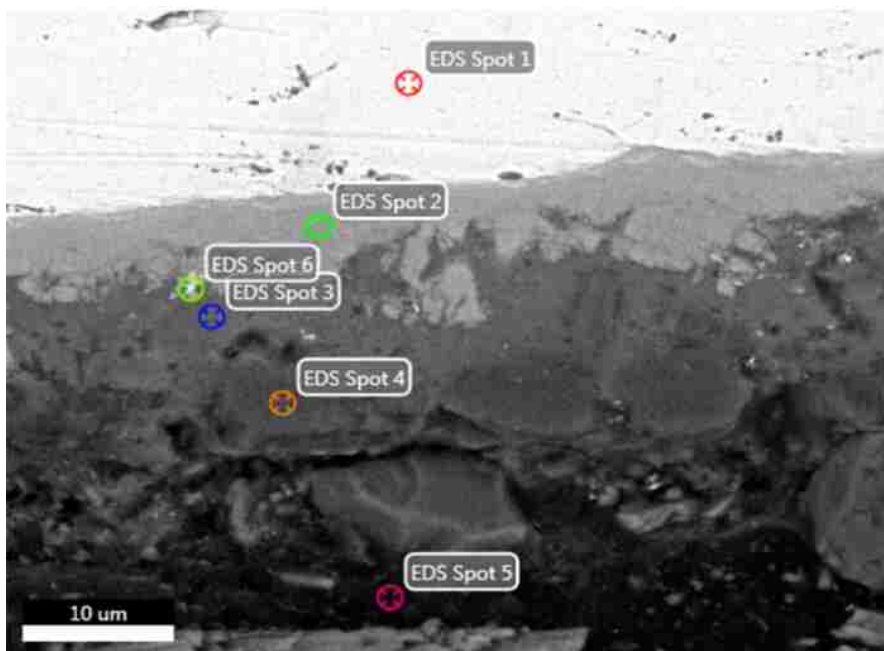
Figure 4.8 SEM result of cross-section of coating (S1 solution).
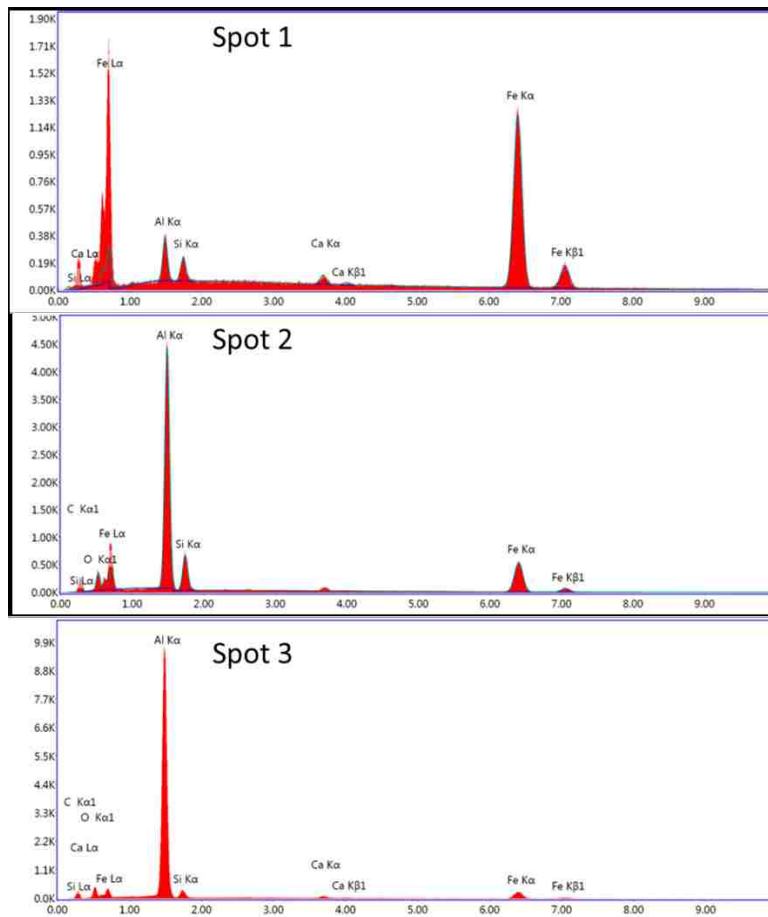
Figure 4.9 EDS analysis results from Spot 1 to Spot 3 in cross-section images of coating (S1) on aluminized steel

4.2 PEO coatings on aluminized AHSS

The PEO coating is prepared on aluminized AHSS. Those aluminized AHSS samples are derived from heated aluminized steel. As mentioned in 3.1 (sample preparation), a number of the square samples were heated in a furnace to 400°C or 900°C for 10 minutes. The heated samples were then placed on a large steel plate for fast cooling in air. The general corrosion behaviors of coatings on aluminized AHSS are analyzed by polarization corrosion test. According to the test results, the general corrosion performance of coating is weakened on aluminized AHSS perhaps due to the iron diffusion.

The potentiodynamic polarization curves of aluminized AHSSs and PEO-coated aluminized AHSSs samples are shown in Figure 4.10. Table 4.2 lists the corrosion potentials, corrosion current density, and curve Tafel slopes (βa and βc) obtained from the graphs. According to the linear polarization theory, the polarization resistance (Rp) is determined by the above corrosion equation. PEO-coated specimen all showed a higher polarization resistance, higher corrosion potential and lower current density compared with their corresponding samples without a PEO coating. Among those three steel samples (without PEO coatings), aluminized AHSS (treated at 900℃) exhibited the lowest corrosion resistance with value of 2180Ω·cm-2. With PEO coatings formed on the tops of aluminized steel and AHSS, the aluminized AHSS base material treated at 400℃ showed the highest polarization resistance of 19000 Ω·cm-2 and the lowest corrosion current of 5.01 E-4 mA.
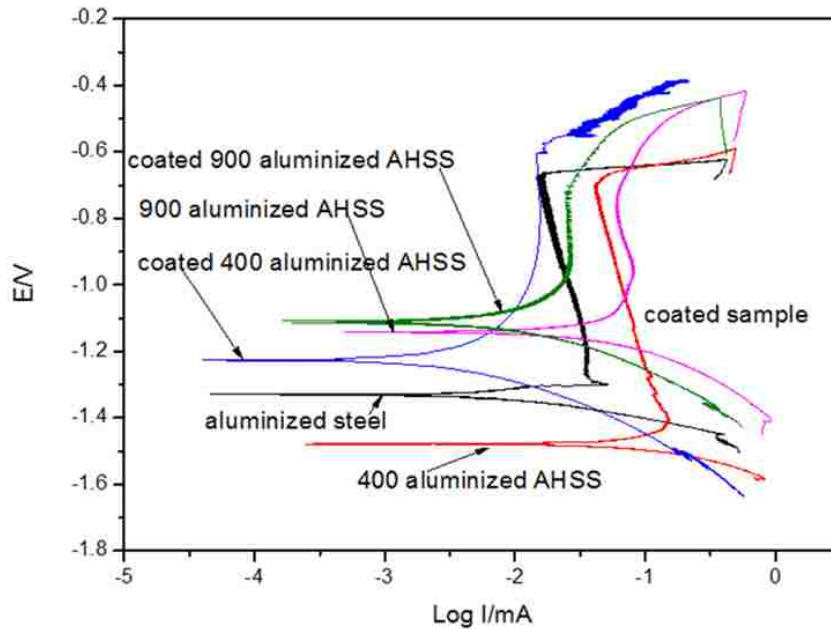
Figure 4.10 Potentiodynamic polarization curves of coatings on stove samples (room temperature, 400℃ and 900℃).

Table 4.2 Potentiodynamic polarization corrosion test results of coatings on aluminized AHSS steel in 3.5% NaCl solution.

	Ecorr(V)	Icorr(mA)	βa(mV)	βc(mV)	Rp(Ω·cm-2)
Coated aluminized AHSS(900℃)	-1.1	7.94 E-4	28.2	79.3	11300
Aluminized AHSS(900℃)	-1.12	3.16 E-3	20.1	75.5	2180
Coated aluminized AHSS(400℃)	-1.22	5.01 E-4	30.3	80.3	19000
Aluminized AHSS(400℃)	-1.5	4.01 E-3	28.2	79.6	2258
Aluminized steel	-1.32	9.77 E-4	23.6	78.3	8070

The cross section morphology of aluminized AHSS is shown in Figure 4.11, where images (a) and (b) are the aluminized AHSS before and after heat treatment respectively. Line scan of EDX was used to analyze the element composition in cross section zone. The graphs on the SEM picture illustrate four principle elements of the layers in cross section: iron, aluminum, oxygen and silicon. As we can see from the SEM pictures, the cross section shows two layers on iron substrate (i.e., diffusion layer and aluminum layer). The total thickness of the layers on aluminized AHSS (heat treated) is about 15microns, 5 microns thicker than the layers above aluminized steel. Also there is a decline of aluminum weight percentages under the aluminum layer. To the contrary, the amount of iron increases. It can suggest that the heat treatment increases substrate iron diffusion to aluminum layer so there is a wider diffusion layer of aluminized AHSS in figure 4.6 (a). The diffusion layer in aluminized AHSS was 7 microns while only 2 microns thick diffusion layer exited in aluminized steel (without heat treatment). The corrosion resistance consistently matches this result. Aluminized AHSS has a lower corrosion resistance than the aluminized steel. Since the aluminum and alumina layer protects the substrate iron

from corrosion and iron is easier to corrode, iron diffusion toward surface would increase the corrosion of layers above substrate.
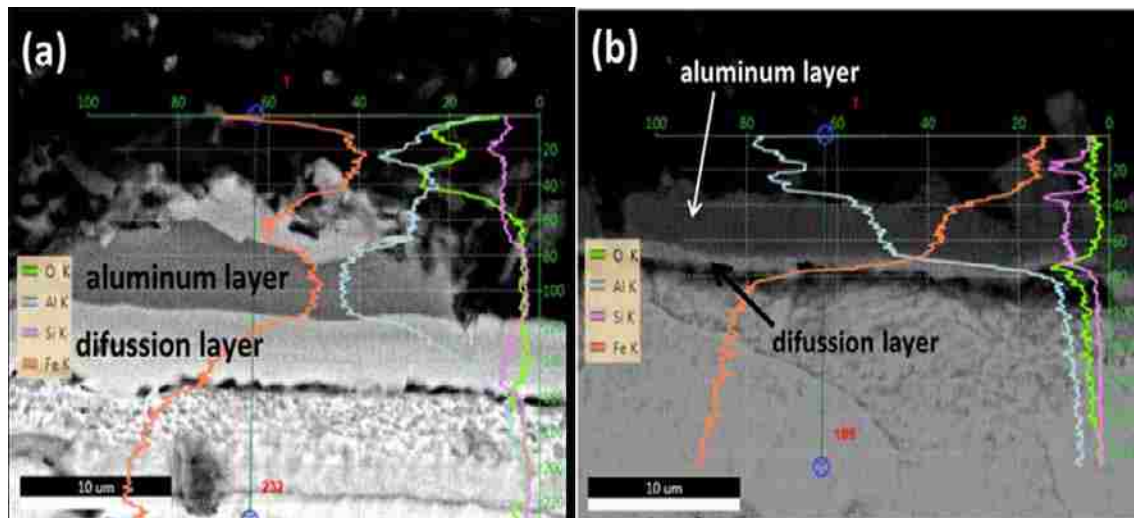
Figure 4.11 EDX analysis of line scan for cross section of sample and SEM micrographs using back-scattered electron mode showing the polished cross-section of coatings on stove samples:(a) aluminized AHSS sample heated at 900 ℃ (b) aluminized AHSS before heat treatment.(X axis: weight percentages of principle elements; Y axis: The positions from the start of line scan).

4.3 PEO coatings on magnesium

PEO coatings are deposited on magnesium with different coating process parameters. The coating treatment time is 6min, 12min and 18min respectively. The coating current modes (table 3.1) include unipolar current mode and bipolar current mode. The general corrosion behavior of coatings on magnesium alloys are studied by polarization corrosion test. Usually, bipolar samples have higher corrosion resistance than unipolar samples when treatment time is constant, and longer treatment time increases the corrosion resistance of coatings. This section is to investigate the prepared coatings on Mg alloys and see if the general trend is followed.

65

Figure 4.12 illustrates the potentiodynamic polarization curves of uncoated Mg alloy and PEO coated specimens by using unipolar or bipolar current modes. The corrosion potentials (E_{corr}), corrosion current density (I_{corr}) and anodic/cathodic Tafel slopes βa and βc are derived from the test data. Based on the approximately linear polarization of the corrosion potential, the polarization resistance (R_p) can be determined. The results are reported in table 4.3.
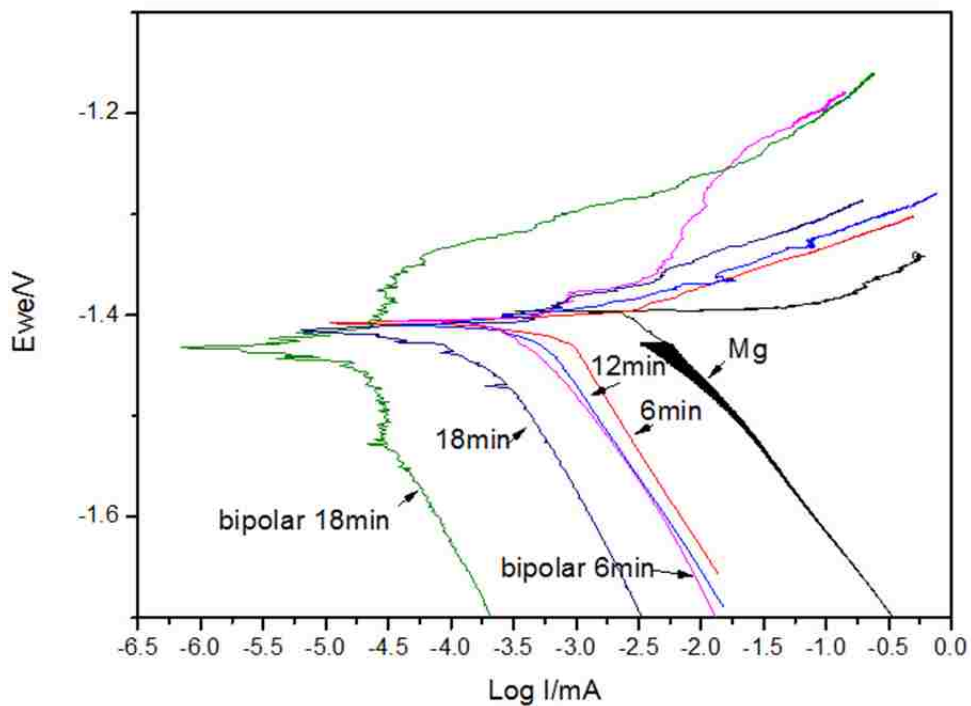
Figure 4.12 Potentiodynamic polarization curves of uncoated Mg sample, coated Mg samples using unipolar (6min, 18min) and using bipolar (6min, 12min, 18min) current modes.

Table 4.3 Potentiodynamic polarization corrosion test results of coatings on magnesium in 3.5% NaCl solution

	E_{CORR}(V)	I_{CORR}(mA)	βa(mV)	βc(mV)	Rp(Ω·cm-2)
Mg	-1.400	2.709E-03	2	124.9	315.9323
U6	-1.415	4.17E-04	34.5	181.1	30215.16
U12	-1.406	3.03E-04	24.5	179.2	30927.34
U18	-1.401	1.37E-04	39.8	165.7	101846.3
B12	-1.42	1.38E-04	55	181.9	133052.6
B18	-1.432	1.1E-06	61.1	196.1	1841312

The uncoated Mg sample shows the lowest corrosion polarization resistance and highest corrosion current. The corrosion resistances of Mg samples coated with unipolar current modes are higher than that of uncoated sample. The corrosion resistance of unipolar treated sample with 18-min treatment time is up to101846.3 Ω, which is much higher than the resistance of uncoated substrate (315.9Ω). The samples with bipolar current modes (B6-B18) exhibit even higher corrosion resistance and lower current densities than the samples treated with unipolar current modes. The reason may be that the unipolar mode likely cause more porous structure which can result in a relatively larger contact area between magnesium and electrolyte. According to plasma discharging model, strong discharge B starts from the bottom of the coating and the discharges A and C are more likely to occur on the upper and top layers. The properties of the plasma discharges in the bipolar current mode are different from that of the unipolar. The bipolar mode can promote the A and C discharge and decrease strong B discharge which can reduce the porous structure on the coating surface.

With the increase in PEO treatment time, higher corrosion resistances were noted on the coatings prepared using either unipolar or bipolar current modes. A thicker coating presented a better corrosion resistance.

4.4 ZRA test results: aluminized steel/coated magnesium and aluminized AHSS/coated magnesium

The general corrosion behaviors of coatings on three substrate materials (aluminized steel，aluminized AHSS and magnesium alloys) were obtained from polarization corrosion test （4.1~4.3）. In 4.4, galvanic corrosion behaviors of galvanic couples between magnesium and steel samples (aluminized steel and aluminized AHSS) is analyzed by zero resistance ammeter （ZRA）corrosion test and boiling test. The galvanic corrosion behavior is explained in terms of anode/cathode area ratio and potential gap (ΔE).

According to the standard EMF series of metals, the electrode potential of magnesium (-2.363 volts) is lower than iron (-0.44 volts). Hence, magnesium is more anodic and appears to be sacrificed in ZRA test even there is PEO coating on it. So the anode/cathode area ratio is coated magnesium/ coated steel samples area ratio namely.

Gibbs free energy change ΔG of a Galvanic cell equals the negative of the number of faradays n passing through the cell, when the reaction takes place, times the Faraday constant F times the electromotive force E of the cell, the above can summarized as the equation $\Delta G = n F \Delta E$. When the other factors keep constant, the potential gap (ΔE) between anode material and cathode material decides the corrosion extent of galvanic couple.

4.4.1 Galvanic combination of aluminized steel or PEO-coated aluminized steel with magnesium or coated magnesium

In the ZRA test, potential difference can result in a current flow at the anodic electrode (magnesium and coated magnesium). In Figure 4.13, the current of bipolar mode treated samples (B6 and B18) are lower than that of magnesium. That indicated that coating can reduce the corrosion in galvanic couples of steel and coated magnesium samples. Moreover, the relatively lower current of bipolar mode treated samples again suggests the impact of plasma discharge during the coating process. The unipolar current modes usually produce strong discharges, which can increase the porosity and pore size in the coating on samples. The unipolar treated samples have larger holes compared to bipolar treated samples, which also increases the contact opportunity between corrosive solution and substrate magnesium. A larger contact area means a higher circuit current.

Additionally, unipolar samples and magnesium have similar current trends in the graph. During the early stage, the corrosive current is between the ranges of 0.005-0.007 mA. Then, it decreases steadily before reaching the range of 0.003 and 0.004 mA. The potential gap between aluminized steel and magnesium is about 0.08V. The maximum current in ZRA test of galvanic couple is 0.007 mA may be due to small value of driving force (ΔE). The corrosive current keeps constant after that. The trend is because of the reaction products which accumulated on the magnesium surface even when the holes connecting magnesium and coating are blocked. Thus, reaction speed was decreased when corrosion happened.

Figure 4.13 ZRA curves of combinations of aluminized steel/ coated magnesium using unipolar (6min, 18min) and using bipolar(6min, 18min) current modes.

The current changing trend of galvanic couples including PEO-coated aluminized steel and coated magnesium samples is shown within 4 hours in Figure 4.14. The corrosion current of magnesium is lower than that of coated samples (U6, U18, B6 and B18). Noticeably, this result is different from the cases of the previously mentioned couples (aluminized steel/coated magnesium), which must be due to the PEO coating that has been deposited on cathode material (aluminized steel). The PEO coating on aluminized steel had increased the corrosion potential and thus corrosion driving force that would change their corrosion behaviors to some degree. In the galvanic couple, PEO-coated aluminized steel and PEO-coated magnesium are supposed to be cathode and anode respectively due to their substrate material electrode potentials. The actual potential difference can also be seen from the potentiodynamic polarization corrosion test curves above. On the one hand, the PEO

70

coating on aluminized steel has increased the corrosion driving force of the coupling. On the other hand, according to the area effect of corrosion theory, the cathode with the insulating coating would be a desired situation. The benefit can be found by comparison corrosion currents of PEO-coated aluminized steel vs Mg (0.0033 mA in Fig 4.14) with aluminized steel vs Mg (0.0038 mA in Fig 4.9). However, if the anode side was taken into consideration, the anode surface should be bigger or less coated to yield better anti-corrosion results if two dissimilar metallic contacts both have an insulation (oxide in this study) coating on their surfaces. As a result, the coated Mg prepared at 6 min under unipolar mode (relatively inferior coating quality) shows a low corrosion current in figure 4.14.
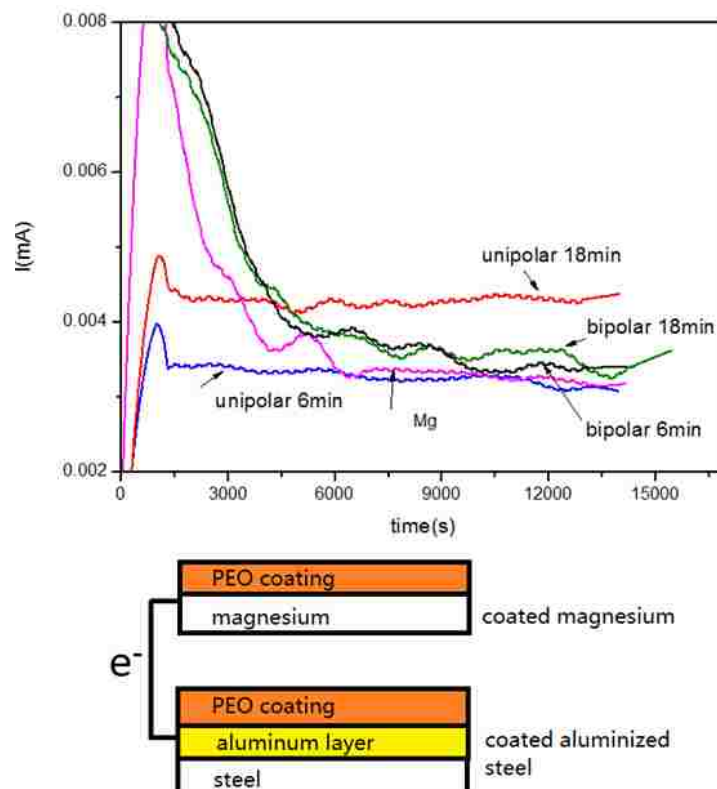
Figure 4.14 ZRA curves of combinations of PEO-coated aluminized steel/PEO-coated magnesium using unipolar (6min, 18min) and using bipolar (6min, 18min) current modes.

71

4.4.2 Galvanic combination of aluminized AHSS/coated aluminized AHSS and

magnesium/coated magnesium

The current changes versus time for galvanic couples including aluminized
AHSS/coated AHSS and coated magnesium samples are illustrated in figure 4.15 and
figure 4.16. As shown in the graphs, the current of galvanic circuit increases a lot
compared with previous galvanic couples whose cathode material is aluminized steel
(without heat treatment). The current was used to be in range of 0.003-0.007 mA.
Now the current has changed to a range of 0-0.01 mA. The dramatic change might be
related to corrosion potential difference. The potential difference is the driving force
of galvanic corrosion. The cathode substrate material in figure 4.15 and figure 4.16 is
aluminized AHSS, and the previous is aluminized steel. According to Table 4.3, the
potential difference between aluminized AHSS and magnesium is 0.28V, much higher
than the potential difference between aluminized steel and magnesium (0.06 V). The
greatly increased potential seems to be able to strike both the uncoated and PEO-
coated Mg samples so efficiently that the corrosion currents were very high.

For the case of PEO-coated Mg, similar phenomena shown in figure 4.16 can also
be observed. When the coupling materials have an oxide insulating layer on their
surfaces, the anode should be bigger or less coated to have a preferential surface area
ratio (i.e., a large ratio of anode/cathode surface area). More porous coatings (large
actual surface area) prepared by a unipolar mode of the PEO process would have a
preferential surface ratio. Therefore, in these ZRA tests, unipolar mode coated Mg
samples outperformed the Mg samples coated using a bipolar mode.
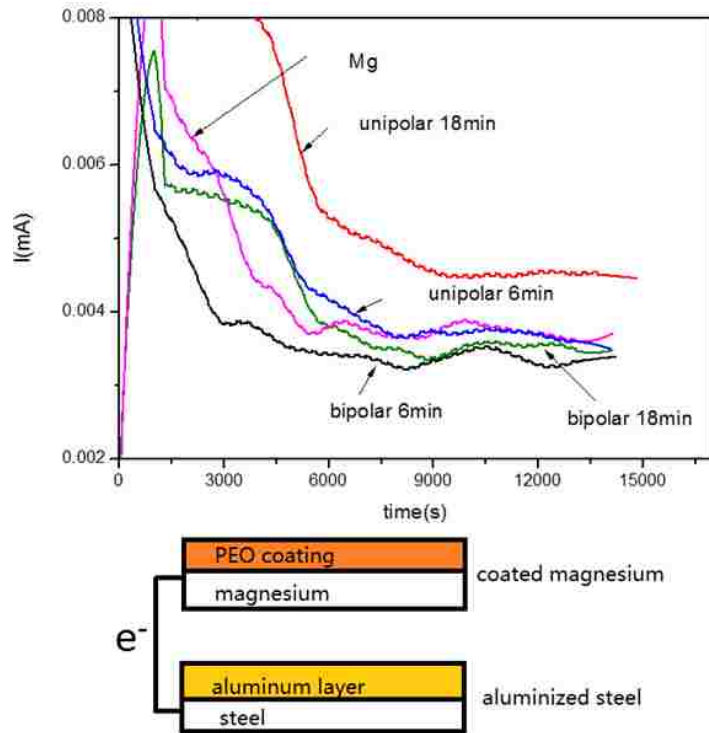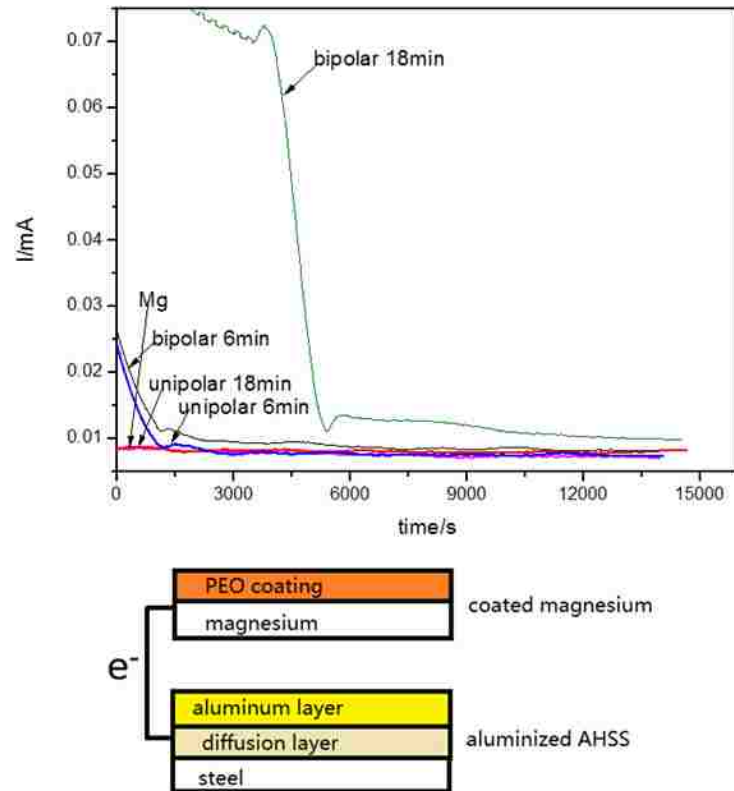
Figure 4.15 ZRA curves of combinations of aluminized AHSS sample/coated magnesium using unipolar (6min, 18min) and using bipolar(6min, 18min) current modes.
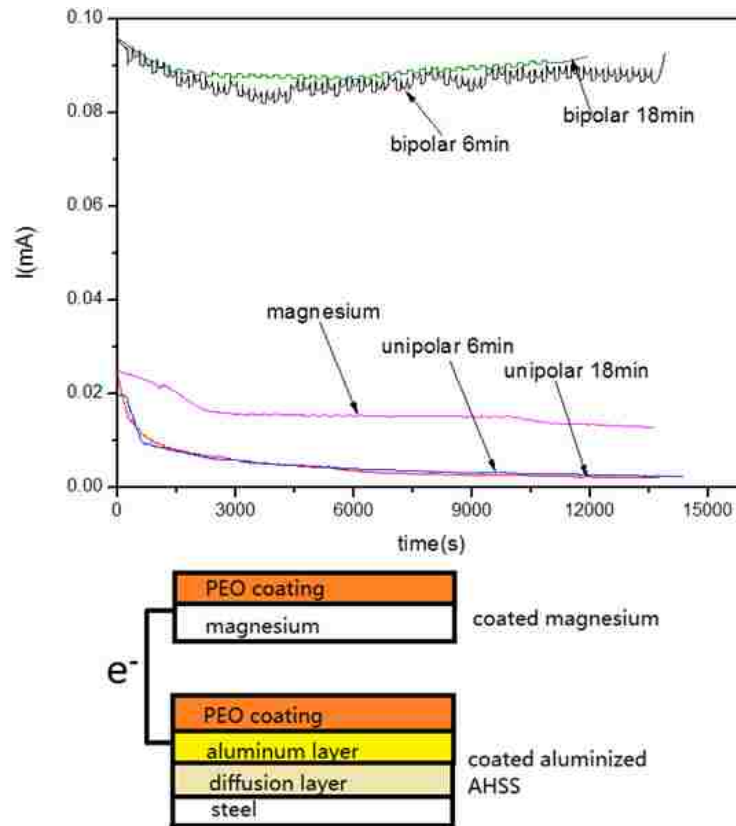
Figure 4.16 ZRA curves of combinations of coated aluminized AHHS / coated magnesium using unipolar (6min, 18min) and using bipolar(6min, 18min) current modes.

4.5 Boiling test results of galvanic couples

4.5.1 Boiling couple of aluminized steel and coated magnesium

4.5.1.1 Corrosion resistance of coatings on magnesium after boiling test.

In the polarization corrosion curves, the unipolar 6min sample has the highest corrosion resistance (86300 $\Omega \cdot cm^{-2}$) and lowest corrosion current (1.583 E-4 mA). It suggests the unipolar 6-min sample corrodes less than the other samples do. And with time increases, corrosion resistance of coated magnesium sample will decrease. The corrosion resistance of unipolar 18-min sample is 32500 $\Omega \cdot cm^{-2}$. The corrosion

current and corrosion potential of unipolar 18-min sample are lower than those of unipolar 6-min sample. This result is different from the corrosion behavior of coated magnesium without boiling test (figure 4.17 and table 4.4). Since the boiling test make samples suffer the galvanic corrosion and the previous polarization corrosion test testify the general corrosion behavior of coated magnesium. The bipolar 6-min sample has a corrosion resistance value of 25900 $\Omega \cdot cm^{-2}$, which is higher than the bipolar 18-min sample with a corrosion resistance value of 6580 $\Omega \cdot cm^{-2}$. All unipolar samples have better galvanic corrosion performance in the galvanic couple of aluminized steel and coated magnesium.
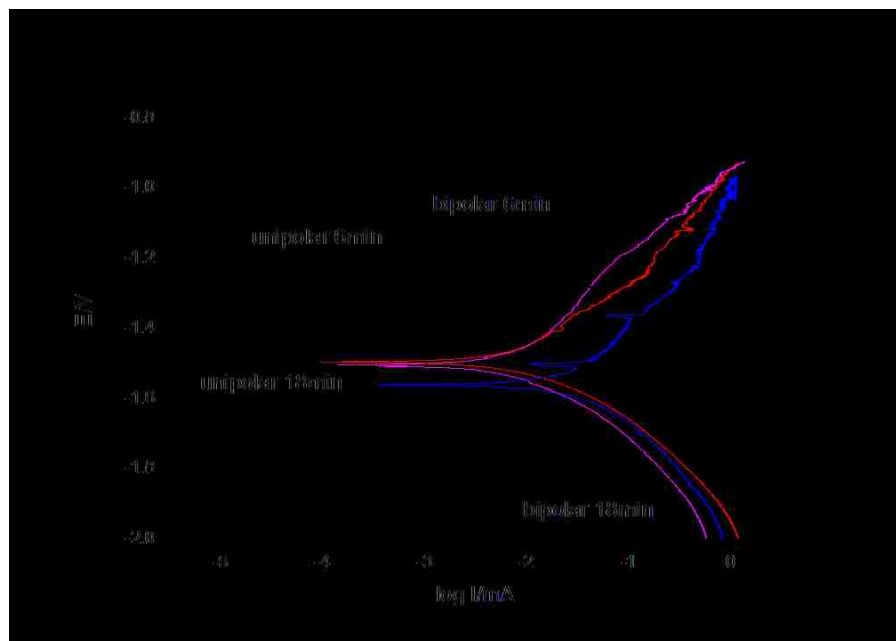
Figure 4.17 Polarization curves of coated magnesium samples after boiling with aluminized steel in corrosive solution for 1 hour.

Table 4.4 Potentiodynamic polarization corrosion test results of coated magnesium in coupling of coated magnesium and aluminized steel after boiling test.

	E_{CORR}(V)	I_{CORR}(mA)	βa(mV)	βc(mV)	$Rp(\Omega \cdot cm^{-2})$
U6	-1.34	1.585 E-4	53.5	76.4	86300
U18	-1.5	3.981 E-4	49.3	75.3	32500
B6	-1.5	5.01 E-4	47.6	80.1	25900
B18	-1.55	1.995 E-4	49.7	76.7	6570

4.5.1.2 Microstructures of the coatings on magnesium after boiling test.

The corrosion behavior is connected closely with the surface morphology of coating. As is shown in figure 4.18, bipolar samples (bipolar 6-min sample and bipolar 18-min sample) have denser coatings than the unipolar samples (unipolar 6-min sample and bipolar 18-min sample). In unipolar 6-min sample, there are more dots and bulk-like surface structure. It is caused by short coating treatment time. Bipolar samples have coating surface with less porosity and holes. R.O. Hussein [72-73] found that the holes on the unipolar samples penetrate deep close to the substrate magnesium. This is due to the strong B-type charge which can be wakened by the bipolar current mode (since the operation modes are mixed with positive and negative current modes). The cross-section images of coated magnesium also suggest that there are two layers above the magnesium substrate, one is outer layer with a significant

amount of connected porosity, cracks and other structural defects, and the other is a more compact inner layer.

When contact the corrosion solution, unipolar outer layer may easily be penetrated. The corrosive electrolyte can touch the inner layer of coating even the substrate surface. As we mentioned in ZRA test, the corrosion performance of metal in galvanic corrosion relates to the anode/cathode area ratio. Coating with more pores that penetrates to the deep can leave the anode coated magnesium a larger contact area, which means a larger anode/cathode ratio compared with bipolar samples. And with longer treatment time, the coating will become thicker. This decreases the anode area to some degree. So U6 and B6 have higher corrosion resistance and lower corrosion current than U18 and B18 do. And with time increases, samples with longer treatment time have fewer holes and smaller porosity.
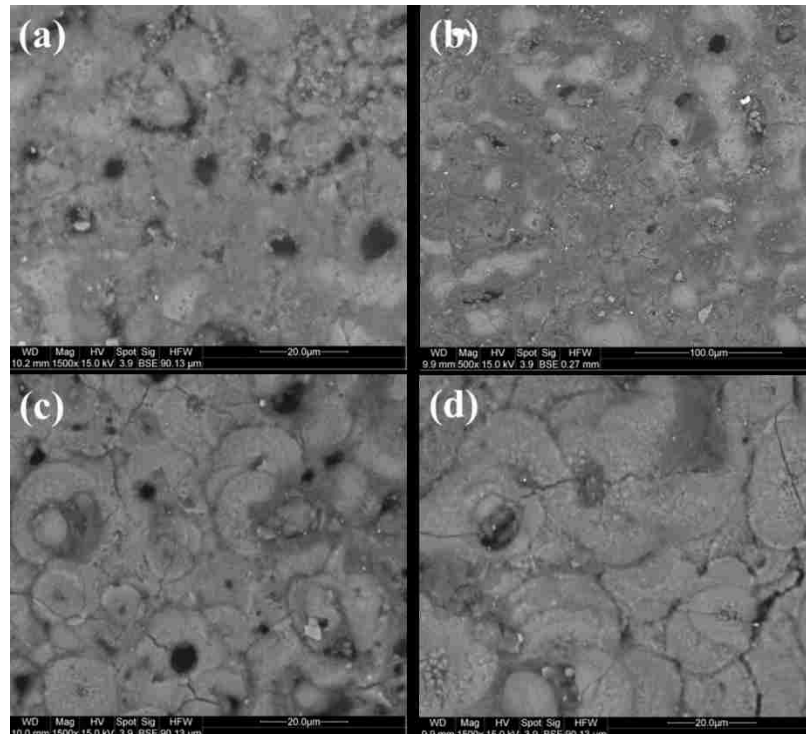
Figure 4.18 SEM micrographs (1500x) using back-scattered electron mode showing the surface morphologies of coated magnesium in boiling couples (coated magnesium

vs aluminized steel): (a) unipolar 6min (b) unipolar 18min (c) bipolar 6min (d) bipolar 18min.

4.5.1.3 Corrosion extent of coatings on magnesium after boiling test.

Although the bipolar samples have fewer pores, the corrosion extent of all coated samples (shown in figure 4.19) is different from ranking in surface morphology of coated samples. Obviously the bipolar samples corrode more in comparison of correspond unipolar samples. From the optical micrographs, bipolar 6-min sample have more cracks and dots on its surface compared to unipolar 6-min coated magnesium. This OM image that shows the corrosion extent matches the result of polarization corrosion test after boiling test. The unipolar 6-sample has highest corrosion resistance. It suggests that it corrodes less in galvanic couple of aluminized steel and coated magnesium. And this research focus on the galvanic corrosion of magnesium coupled with steel samples with different coating layers. So the behavior of magnesium without aluminized coupling is also studied.
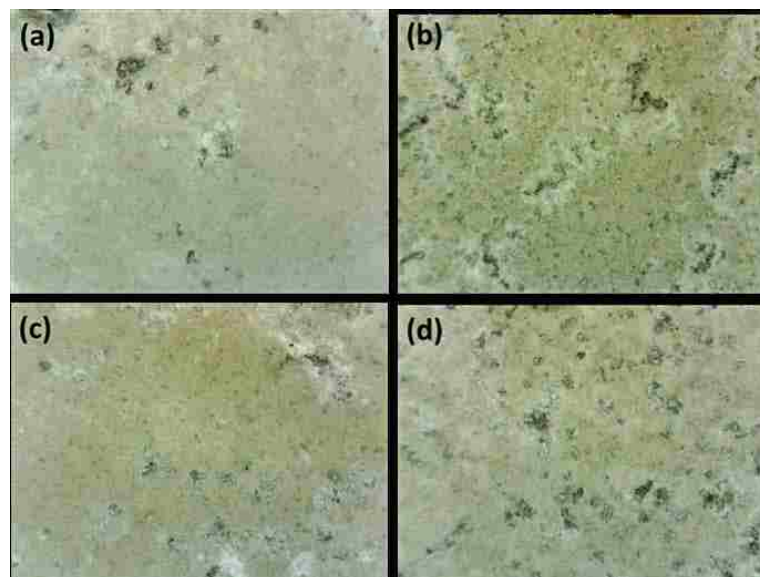
Figure 4.19 Optical microscope picture of coated magnesium after boiling test:
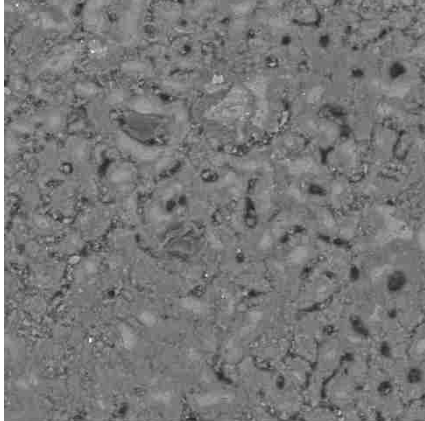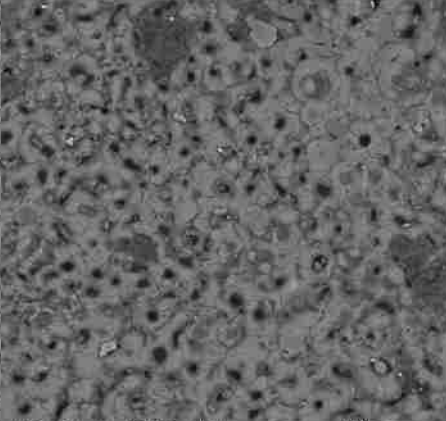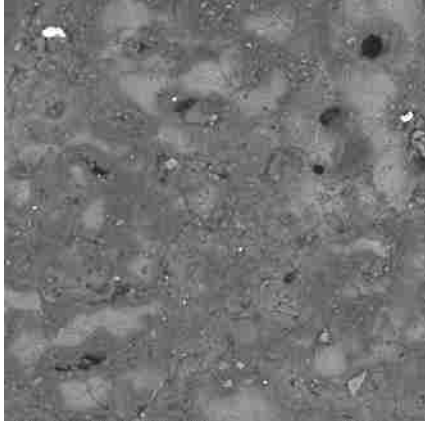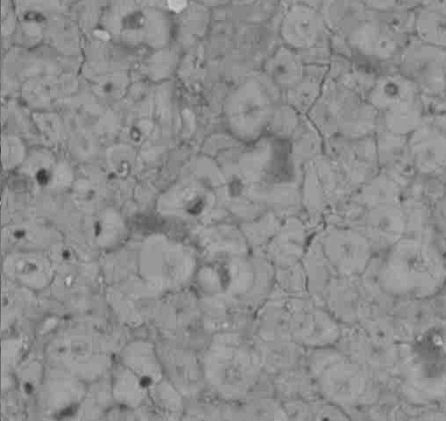
(a) unipolar 6min, (b) unipolar 18min, (c) bipolar 6min, (d) bipolar 18min.

4.5.1.4 Average porosity of coatings on magnesium after boiling test.

Table 4.5 shows the SEM micrographs of coating surface on coated magnesium. And the average porosities (which shows the percentage of area that includes porosity). The average porosities are measured according to the SEM micrographs under 500 x magnifications. There are pores of different sizes. The corrosive reaction products exit in some large holes. It can be observed that coating treatment time and current mode can affect the average porosity of coating surface. The pore sizes vary from less than 3μm (small pores) to larger than 10 μm (large pores). Unipolar 6-min sample and unipolar 18-min sample, with average porosity of 6.52% and 3.43% respectively, show a large pore size range (<3μm ~ >10μm). When the coating time increases, there is a decline in average porosity of the coating. And bipolar current mode can decrease the pore size. On the coating surface of bipolar samples, pore size is mostly under 10 μm. The porosity can also be decreased by the bipolar current mode. Bipolar samples have average porosities of 4.91% and 2.75% respectively with the treatment time of 6 minutes and 18minutes.

For the reason of formation of microholes on the coating surface on magnesium, R.O. Hussein et al. [74] mentioned that it was due to oxygen gas trapping and evolution and/or electrolyte vapors. In addition Zhou et al. [80] thought that low pilling-bedworth ratio of magnesium could cause high porosity of PEO coatings on magnesium alloys. The average porosity verifies that unipolar samples have larger holes and higher porosity compared to bipolar samples. Those larger holes provide pathways to the corrosive solution and thus increase the anode/cathode area ratio.

Table 4.5 SEM micrographs showing the surface morphology of PEO coated Mg alloys at different treatment times showing the percentage area of porosity, %.

	Unipolar current mode	Bipolar current mode
6 min		
	6.52%	4.91%
18 min		
	3.43%	2.75%

4.5.1.5 The comparison between Mg (in galvanic couple) and Mg (individual)

In the boiling test, two magnesium samples both suffer the boiling process, one is put in to the corrosive solution independently and the other is magnesium coupled with aluminized steel. The polarization corrosion curves of two magnesium samples are shown in figure 4.20. The corrosion current of two samples are close but there is a little difference in the potential. Individual magnesium has higher corrosion potential

(-1.55 V) than the galvanic magnesium (-1.52 V) does. The corrosion current of individual magnesium sample and galvanic magnesium sample are 7.94 E-3 mA and 7.53 E-3 mA respectively. The magnesium corrodes less after the boiling test while the difference is not obvious. The galvanic magnesium is to be the anode in the couple of magnesium and aluminized steel. The galvanic magnesium will suffer not only general corrosion but also galvanic corrosion. The coating can prevent galvanic corrosion according to corrosion current in table 4.3. The corrosion current of unipolar 6-min sample is 1.58 E-4 Ma, which is lower than the pure magnesium coupled with aluminized steel. In a result, the coating can both prevent general corrosion and galvanic corrosion.
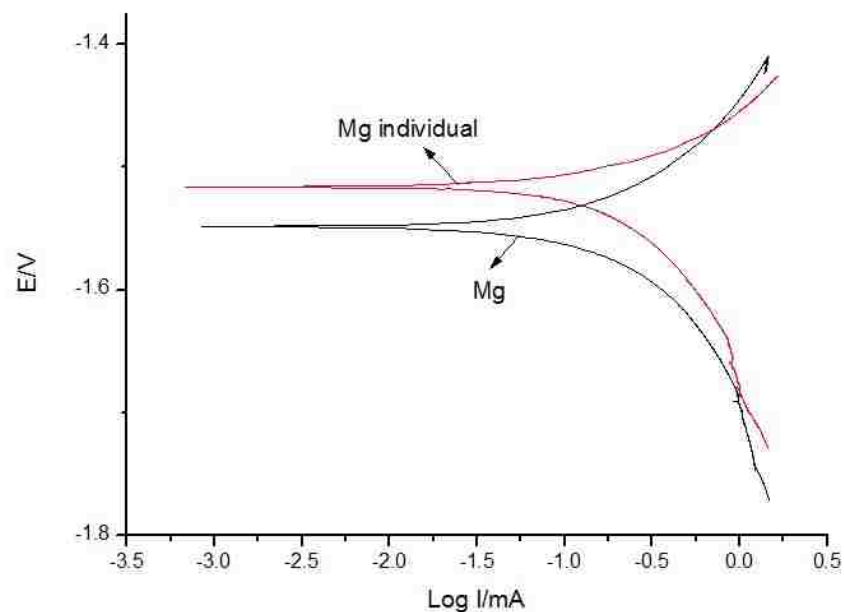
Figure 4.20 Polarization corrosion curves of individual magnesium and galvanic magnesium after boiling test.

Figure 4.21 shows the surface OM images of individual magnesium sample and galvanic magnesium sample. The coating surfaces of two samples both have corrosion traces. But it can be seen that the corrosion area does not cover the whole surface of

magnesium in the individual magnesium sample. However, the coating surface of coupling magnesium is covered by the corrosion traces. This may be due coupling magnesium sample needs to suffer not only general corrosion but also galvanic corrosion. And since magnesium in galvanic couple is to be sacrificed, the coupling aluminized steel has fewer corrosion cracks and dots on its surface after boiling test. The individual aluminized steel sample has more corrosion traces. The difference between surface situations of two aluminized samples is caused by the protection mechanism in galvanic corrosion. The aluminized steel is more cathodic and protected by the galvanic magnesium.
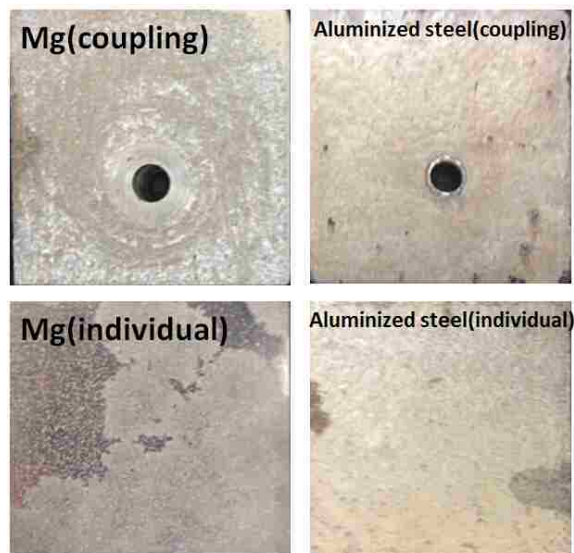
Figure 4.21 Surface OM images of individual magnesium and galvanic magnesium after boiling test.

4.5.2 Boiling couple of coated aluminized steel and coated magnesium

4.5.2.1 Corrosion resistance of coatings on magnesium after boiling test.

Figure 4.22 shows the polarization corrosion curves of coated magnesium after boiling test. Unipolar 6-min sample has better corrosion performance that it has the

highest corrosion resistance (1738000 Ω·cm-2) and lowest corrosion current (7.94 E-6 mA). Corrosion resistance of coated magnesium sample will descend when the coating treatment time increases. The corrosion resistance of unipolar 18-min sample is 168900 Ω·cm-2. The bipolar 18-min sample has a corrosion resistance value of 130900 Ω·cm-2, which is lower than the bipolar 6-min sample with a corrosion resistance value of 129200 Ω·cm-2. All unipolar samples have better galvanic corrosion performance in the galvanic couple of coated aluminized steel and coated magnesium compared to bipolar samples. As mentioned in first coupling (coated magnesium and aluminized steel). Corrosion curves of coated magnesium do not follow the same trend as coated magnesium without boiling test (figure 4.7 and table 4.2). Since the previous samples do not suffer the boiling test, it is analyzed to show the general corrosion behavior of coatings.

Table 4.6 Corrosion polarization test results of coated magnesium in coupling of coated magnesium and coated aluminized steel after boiling test

	E_{CORR}(V)	I_{CORR}(mA)	βa(mV)	βc(mV)	$Rp(\Omega \cdot cm^{-2})$
U6	-1.28	7.94 E-6	52.6	80.1	1738000
U18	-1.29	7.94 E-5	52.3	75.2	168900
B6	-1.32	1 E-4	48.7	76.3	129200
B18	-1.32	1 E-4	50.1	75.4	130900
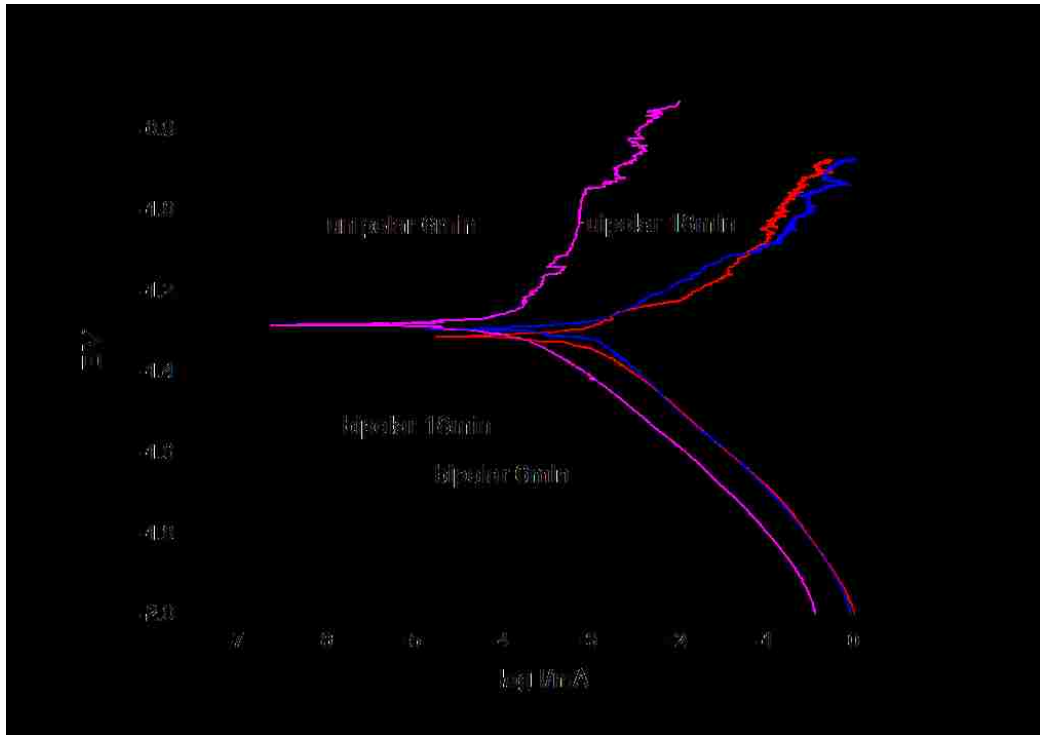
Figure 4.22 Polarization curves of coated magnesium samples after boiling with coated aluminized steel in corrosive solution for 1 hour.

4.5.2.2 Microstructures of the coatings on magnesium after boiling test.

Surface morphology significantly influences the properties of coatings. The corrosion behavior is decided by the coating surface. In figure 4.24, the SEM micrographs of magnesium coating surface after boiling test are introduced. As we discussed before, bipolar samples have fewer holes and lower pore density. When contact the corrosion solution, unipolar outer layer may easily be penetrated since unipolar samples have larger holes. The corrosive electrolyte can contact with inner layer of coating even the substrate surface. The outer layer of coating that uses bipolar mode is hard for corrosive solution to break. It may be due to the strong B-type charge as mentioned in paper of R.O. Hussein [72-73]. The good quality of coatings using bipolar mode also means a smaller anode/cathode area ratio
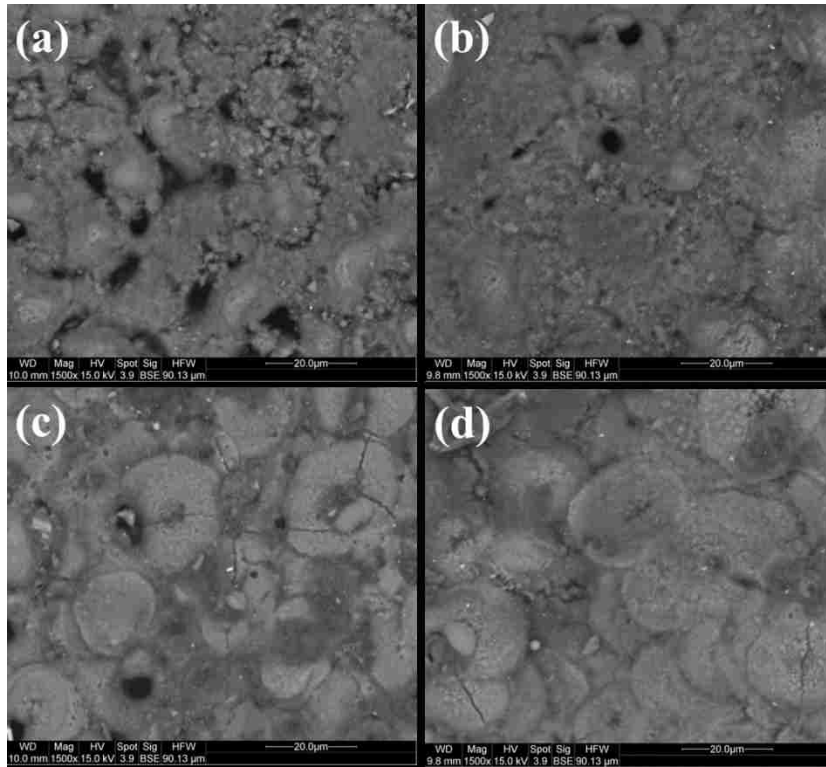
Figure 4.23 SEM micrographs using back-scattered electron mode showing the surface morphologies of coated magnesium in boiling couples (coated magnesium vs coated aluminized steel): (a) unipolar 6min (b) unipolar 18min (c) bipolar 6min (d) bipolar 18min.

4.5.2.3 Corrosion extent of coatings on magnesium after boiling test.

The corrosion performance of metal in galvanic corrosion relates to the anode/cathode area ratio. A larger anode/cathode area ratio is preferable in the galvanic couplings. According to the ZRA test and boiling test, unipolar samples are more desirable than bipolar samples since they have relatively larger anode/cathode area ratio with steel samples. And with longer treatment time, the coating will become thicker. This decreases the anode area to some degree. So samples with shorter treatment time are also better in the galvanic couples.

Although the bipolar samples have fewer pores, the corrosion extent ranking (shown in figure 4.24) is different from the ranking in surface morphology of coated samples. Obviously the bipolar samples corrode more in comparison of correspond unipolar samples. This result matches the corrosion resistance of coated magnesium. But time effect is not obvious on those coated magnesium.
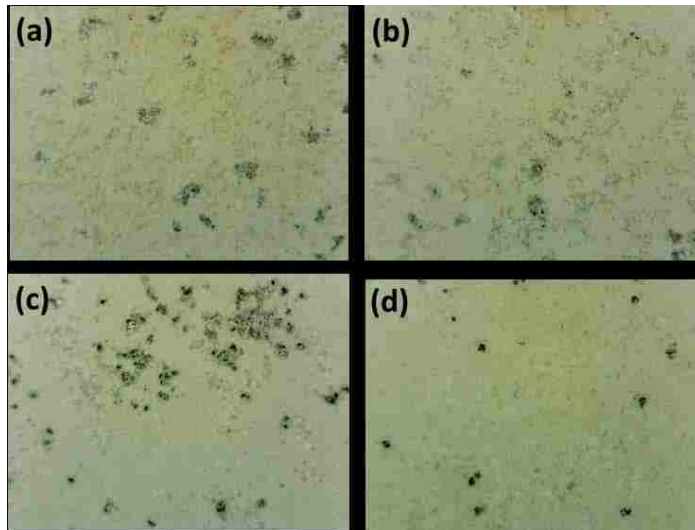
Figure 4.24 Optical microscopy pictures of coated magnesium after boiling test:

(a) unipolar 6min, (b) unipolar 18min, (c) bipolar 6min, (d) bipolar 18min.

4.6 Summary

PEO coatings are deposited on the surface of three substrate materials (aluminized steel, aluminized AHSS and magnesium). Potentiodynamic polarization corrosion test and other characterization methods are utilized to study the anti-general corrosion performance. Galvanic couples consist of those coated samples. The magnesium/coated magnesium are to be anode and steel/coated steel samples are to be cathode. ZRA test, boiling test and other characterization methods are used to investigate the ability of anti-galvanic corrosion.

For coated aluminized steel, coating treatment time is a critical factor that it affects the corrosion resistance and surface morphology; For coated aluminized AHSS, the heat treatment time is influential. It promotes the iron diffusion to coating surface; For coated magnesium, current mode and coating time both make an effect on the anti-general corrosion behavior. Longer treatment time and bipolar current mode is good for higher corrosion resistance.

For galvanic couples of aluminized steel/ coated magnesium and coated aluminized steel/ coated magnesium, the anti-galvanic corrosion behaviors are evaluated in terms of potential gap (ΔE) and anode/cathode area ratio. In ZRA test, 6-min bipolar coated magnesium/ aluminized steel and 6min-unipolar coated magnesium perform better in preventing galvanic corrosion. The galvanic current is in range of 0.003-0.007 mA due to the potential gap of 0.08V. In boiling test, 6-min unipolar coated magnesium performs better in both galvanic couplings.

For galvanic couples of aluminized AHSS/coated magnesium and coated aluminized AHSS/coated magnesium, the anode/cathode area ratio and potential gap influence the ability of coatings for preventing the galvanic corrosion. In ZRA test, the galvanic current is lowest when the anode is 6-min unipolar coated magnesium in both galvanic couples. The galvanic current is in range of 0–0.01mA due to relatively larger potential gap value (0.28V).

In general, the PEO coatings on all three substrate can help prevent general corrosion. 6-min coated magnesium with unipolar current mode performs best in most galvanic couplings for preventing both general corrosion and galvanic corrosion.

Chapter 5: CONCLUSIONS AND FUTURE WORK

In this study, Plasma Electrolytic Oxidation (PEO) was used to produce coatings on aluminized steel, heated aluminized steel and magnesium. Different electrolyte plans were used in PEO coating deposition. The factors (treatment time and current modes) are discussed about the corrosion properties of coatings on three substrate materials. For aluminized steel, the treatment time was 1min, 2min, 3min and 4min respectively. For magnesium, the coating time was 6min, 12min and 18min respectively. General corrosion behavior of coatings was analyzed by polarization corrosion test. Galvanic corrosion behavior of coatings was studied by ZRA test and boiling test. **Galvanic couples** were aluminized steel/ coated magnesium (U6, U18, B6 and B18), coated aluminized steel(3-min)/ coated magnesium (U6,U18, B6 and B18), heated aluminized steel/ coated magnesium (U6, U18, B6 and B18) and coated heated aluminized steel (3-min)/coated magnesium (U6, U18, B6 and B18).Other characterization methods were utilized to help examine the surface morphology.

5.1 PEO coating on aluminized steel

Pin-on-disc tribotest was used to study the wear resistance and COF of oxide coating of uncoated sample and coated sample with different treatment time. The sample with 3-min treatment time has a better wear performance than both the uncoated sample and 1-min coated sample. The PEO treatment didn't change much of surface roughness of the samples.

The potentiodynamic polarization corrosion test was utilized to study corrosion resistance of the coating surface. Compared to the uncoated sample and coated sample with shorter treatment time, the 3-min coated sample has a lower corrosion current density and higher corrosion resistance (261000 $\Omega \cdot cm^{-2}$). This indicates the better

corrosion resistance of oxide coating can be prepared at the longer (3 min) treatment time.

The temperature difference between the surfaces of the tested samples indicates that the PEO-coated sample has better thermal absorption and emissivity properties.

5.2 PEO coatings on aluminized AHSS

PEO-coated specimen all show a higher polarization resistance, higher corrosion potential and lower current density compared with their corresponding samples without a PEO coating. The corrosion resistance of coating on aluminized AHSS is lower than that of aluminized steel maybe due to the iron diffusion into Al layer in intermetallic layer of aluminized steel. Iron diffusion layer above steel in aluminized AHSS is 5 microns thicker than that in aluminized steel. This diffusion layer is easier to corrode.

5.3 PEO coating on magnesium

Current modes and time significantly affect corrosion behaviors of coatings on magnesium. Both modes improve the corrosion resistance as compared to the uncoated alloy. The coating prepared using bipolar current modes have higher corrosion resistances compared to unipolar treated samples. Longer treatment time increases the coating thickness thus improves the corrosion behaviors. Bipolar current mode helps decrease average porosity on the coating surface and pore size. In general, 18-min coated magnesium with bipolar current modes have highest corrosion resistance (1841312 $\Omega \cdot cm^{-2}$) among those coated magnesium samples.

5.4 Galvanic corrosion of galvanic couples

Coated magnesium is supposed to be the anode and steel samples are to be the cathode. From anode/cathode area ratio, a PEO coating on Mg can slow down the general corrosion but it may cause an unfavorable surface area ratio of anode to cathode for the case of galvanic coupling. In galvanic corrosion couplings, a relatively low quality PEO coating prepared at unipolar mode seems a good compromising in protection from both general and galvanic corrosion. The reason for this seems that more porous surface structure would increase anodic surface area and thus offer a preferential surface area ratio of anode vs cathode.

When the cathode is aluminized steel or coated aluminized steel, 6-min bipolar coated magnesium/ aluminized steel and 6min-unipolar coated magnesium perform better for preventing galvanic corrosion in ZRA test. The galvanic current is in range of 0.003-0.007 mA due to the potential gap of 0.08V. In boiling test, 6-min unipolar coated magnesium performs better in both galvanic couplings due to the larger anode/cathode area ratio. The unipolar samples have larger holes and higher porosity compared to the bipolar samples.

When the cathode is aluminized AHSS or coated aluminized AHSS, the galvanic current is lowest when the anode is 6-min unipolar coated magnesium in both galvanic couples in ZRA test. The galvanic current is in range of 0–0.01 mA. Since potential gap (0.28V) between aluminized AHSS and magnesium is higher compared to the galvanic couple whose cathode is aluminized steel.

When the driving force is high, the surface area ratio is a mainly decisive factor, a relatively inferior (in terms of general corrosion prevention) coating (but favourable surface ratio of anode/cathode for galvanic corrosion prevention). (e.g., for 6 min unipolar treated sample) will behave better in galvanic coupling case. When the

corrosion driving force is small (for aluminized steel/ coated magnesium coupling), that is, the potential difference between cathode and anode is small, a coating with a better general corrosion resistance (e.g., for bipolar treated samples) will perform better in a galvanic coupling case.

Therefore, the influence of PEO coatings on galvanic corrosion behaviour of aluminized steel or aluminized AHSS coupling with Mg results from combinative consequence of alterations in corrosion potential difference (driving force) and anode/cathode ratio (area effect) caused by the coatings.

5.5 Future work

Since the galvanic couple are designed to use inside automotive, it is essential to investigate the mechanical properties for coating on aluminized steel. For better anti-corrosion performance, the powder coating above existing PEO coating is preferred in future research. It is necessary to conduct a more detailed analysis on the other electrolyte plans in the PEO deposition process. In addition, the parameters during coating process such as current mode can be introduced in coating process to see their effects on corrosion and mechanical properties.

For galvanic couplings, the other parameters such as alloying element, insulation distance and shapes of anode and cathode can be designed in a more detailed study to find the effects of those parameters on galvanic couplings. Additionally, the relationship between coating time for cathode (steel samples) and corrosion extent can be determined in the future. The practical conditions (extreme high temperature and high pressure) in real applications can also be taken into consideration for next research.

REFERENCES

[1] Tharumarajah, A., & Koltun, P. (2007). Is there an environmental advantage of using magnesium components for light-weighting cars. Journal of Cleaner Production, 15(11), 1007-1013.

[2] Cherubini, F., Raugei, M., & Ulgiati, S. (2008). LCA of magnesium production: Technological overview and worldwide estimation of environmental burdens. Resources, Conservation and Recycling, 52(8), 1093-1100.

[3] Friedrich, H., & Schumann, S. (2001). Research for a "new age of magnesium" in the automotive industry. Journal of Materials Processing Technology, 117(3), 276-281.

[4] Deqing, Wang, Shi Ziyuan, Zou Longjiang, A liquid aluminum corrosion resistance surface on steel substrate, Applied Surface Science 214, no. 1 (2003): 304-311.

[5] Wang, Chaur-Jeng, Shih-Ming Chen, The high-temperature oxidation behavior of hot-dipping Al–Si coating on low carbon steel, Surface and Coatings Technology 200, no. 22 (2006): 6601-6605.

[6] Schneider, M., K. Kremmer, C. Lämmel, K. Sempf, and M. Herrmann. "Galvanic corrosion of metal/ceramic coupling." Corrosion Science 80 (2014): 191-196.

[7] Varela, F. E., Y. Kurata, N. Sanada, The influence of temperature on the galvanic corrosion of a cast iron-stainless steel couple (prediction by boundary element method), Corrosion science 39, no. 4 (1997): 775-788.

[8] Nie, X., L. Wang, E. Konca, A. T. Alpas, Tribological behaviour of oxide/graphite composite coatings deposited using electrolytic plasma process, Surface and Coatings Technology 188 (2004): 207-213.

[9] Cole, G. (1997). A. Glove, R. Jeryan, G. Davies. Steel World, 2(1), 75-83.

[10] http://carnegieendowment.org/files/china_electric_vehicles.pdf

[11] Liu, Y., Liu, Y., & Chen, J. (2014). The impact of the Chinese automotive industry: scenarios based on the national environmental goals. Journal of Cleaner Production.

[12] http://www.drivealuminum.org/research-resources/research

[13] Hirsch, J. (2014). Recent development in aluminium for automotive applications. Transactions of Nonferrous Metals Society of China, 24(7), 1995-2002.

[14] Bartz, W. J. (1993). Aluminum materials technology for automobile construction. London: Mech Eng Publ.

[15] Lumley, R. (Ed.). (2010). Fundamentals of aluminium metallurgy: Production, processing and applications. Elsevier.

[16] Cherubini, F., Raugei, M., & Ulgiati, S. (2008). LCA of magnesium production: Technological overview and worldwide estimation of environmental burdens. Resources, Conservation and Recycling, 52(8), 1093-1100.

[17] Friedrich, H., & Schumann, S. (2001). Research for a "new age of magnesium" in the automotive industry. Journal of Materials Processing Technology, 117(3), 276-281.

[18] http://www.intlmag.org/magnesiumapps/automotive.cfm

[19] Luo, A. A. (2013). Magnesium casting technology for structural applications. Journal of Magnesium and Alloys, 1(1), 2-22.

[20] Das, S. (2003). Magnesium for automotive applications: Primary production cost assessment. JOM, 55(11), 22-26.

[21] Kulekci, M. K. (2008). Magnesium and its alloys applications in automotive industry. The International Journal of Advanced Manufacturing Technology, 39(9-10), 851-865.

[22] Luo, A. A. (2003, February). Recent magnesium alloy development for automotive powertrain applications. In Materials Science Forum (Vol. 419, pp. 57-66).

[23] Luo, A. A. (2002). Magnesium: current and potential automotive applications. jom, 54(2), 42-48.

[24] Blawert, C., Hort, N., & Kainer, K. U. (2004). Automotive applications of magnesium and its alloys. Trans. Indian Inst. Met, 57(4), 397-408.

[25] http://www.engineerstudent.co.uk/die_casting.html

[26] Kuziak, R., Kawalla, R., & Waengler, S. (2008). Advanced high strength steels for automotive industry. Archives of civil and mechanical engineering, 8(2), 103-117.

[27] Llewellyn, D. T., & Hillis, D. J. (1996). Dual phase steels. Ironmaking & steelmaking, 23(6), 471-478.

[28] Kamp, A., Celotto, S., & Hanlon, D. N. (2012). Effects of tempering on the mechanical properties of high strength dual-phase steels. Materials Science and Engineering: A, 538, 35-41.

[29] Granbom, Y. (2010). Structure and mechanical properties of dual phase steels: An experimental and theoretical analysis.

[30] Caseres, L. (2007). Electrochemical behavior of aluminized steel type 2 in scale-forming waters. ProQuest.

[31] Wu, Z., Xia, Y., Li, G., & Xu, F. (2007). Structure and mechanical properties of ceramic coatings fabricated by plasma electrolytic oxidation on aluminized steel. Applied surface science, 253(20), 8398-8403.

[32] Suehiro, M., Maki, J., Kusumi, K., Ohgami, M., & Miyakoshi, T. (2003). Properties of aluminized steels for hot-forming (No. 2003-01-2853). SAE Technical Paper.

[33] Wu, X. Q., Jing, H. M., Zheng, Y. G., Yao, Z. M., & Ke, W. (2004). Study on high-temperature naphthenic acid corrosion and erosion-corrosion of aluminized carbon steel. Journal of materials science, 39(3), 975-985.

[34] LI, H. F., YU, D. Y., & ZHENG, J. S. (2001). Performance and Application of Hot dip Aluminized Steel [J]. Materiais Protection, 5, 009.

[35] Deqing, W., & Ziyuan, S. (2003). Effect of ceramic particles on cell size and wall thickness of aluminum foam. Materials Science and Engineering: A, 361(1)

[36] Deqing, W. (2008). Phase evolution of an aluminized steel by oxidation treatment. Applied Surface Science, 254(10), 3026-3032.

[37] Deqing, W., Ziyuan, S., & Longjiang, Z. (2003). A liquid aluminum corrosion resistance surface on steel substrate. Applied Surface Science, 214(1), 304-311.

[38] Mehrer, H., Eggersmann, M., Gude, A., Salamon, M., & Sepiol, B. (1997). Diffusion in intermetallic phases of the Fe–Al and Fe–Si systems. Materials Science and Engineering: A, 239, 889-898.

[39] Davis, J. R. (Ed.). (1999). Corrosion of aluminum and aluminum alloys. Asm International.

[40] Szklarska-Smialowska, Z. (1999). Pitting corrosion of aluminum. Corrosion science, 41(9), 1743-1767.

[41] Tomcsanyi, L., Varga, K., Bartik, I., Horányi, H., & Maleczki, E. (1989). Electrochemical study of the pitting corrosion of aluminium and its alloys—II. Study of the interaction of chloride ions with a passive film on aluminium and initiation of pitting corrosion. Electrochimica Acta, 34(6), 855-859.

[42] Deshpande, K. B. (2012). Effect of aluminium spacer on galvanic corrosion between magnesium and mild steel using numerical model and SVET experiments. Corrosion Science, 62, 184-191.

[43] Cheng, Y. L., Qin, T. W., Wang, H. M., & Zhang, Z. (2009). Comparison of corrosion behaviors of AZ31, AZ91, AM60 and ZK60 magnesium alloys. Transactions of Nonferrous Metals Society of China, 19(3), 517-524.

[44] Lunder, O., Lein, J. E., Aune, T. K., & Nisancioglu, K. (1989). The role of Mg17Al12 phase in the corrosion of Mg alloy AZ91. Corrosion, 45(9), 741-748.

[45] Hehmann, F., F. H. Froes, and W. Young. "Rapid solidification of alumium, magnesium, and titanium [J]." Journal of Metals 39.8 (1987): 14-21.

[46] Cheng, Y. L., Qin, T. W., Wang, H. M., & Zhang, Z. (2009). Comparison of corrosion behaviors of AZ31, AZ91, AM60 and ZK60 magnesium alloys. Transactions of Nonferrous Metals Society of China, 19(3), 517-524.

[47] https://www.anochrome.com/technical/corrosion-protection-prevention/

[48] Song, G., Johannesson, B., Hapugoda, S., & StJohn, D. (2004). Galvanic corrosion of magnesium alloy AZ91D in contact with an aluminium alloy, steel and zinc. Corrosion Science, 46(4), 955-977.

[49] Liu, C., Chen, D. L., Bhole, S., Cao, X., & Jahazi, M. (2009). Polishing-assisted galvanic corrosion in the dissimilar friction stir welded joint of AZ31 magnesium alloy to 2024 aluminum alloy. Materials Characterization, 60(5), 370-376.

[50] Clark, W. J., Ramsey, J. D., McCreery, R. L., & Frankel, G. S. (2002). A galvanic corrosion approach to investigating chromate effects on aluminum alloy 2024-T3. Journal of The Electrochemical Society, 149(5), B179-B185.

[51] Mansfeld, F., & Kenkel, J. V. (1975). Galvanic corrosion of Al alloys—III. The effect of area ratio.

[52] Mathieu, S., Rapin, C., Steinmetz, J., & Steinmetz, P. (2003). A corrosion study of the main constituent phases of AZ91 magnesium alloys. Corrosion Science, 45(12), 2741-2755.

[53] Do Lee, C., Kang, C. S., & Shin, K. S. (2000). Effect of galvanic corrosion between precipitate and matrix on corrosion behavior of As-cast magnesium-aluminum alloys. Metals and Materials, 6(4), 351-358.

[54] Zhu, L., & Song, G. (2006). Improved corrosion resistance of AZ91D magnesium alloy by an aluminium-alloyed coating. Surface and Coatings Technology, 200(8), 2834-2840.

[55] Lee, Y. H., Zhang, X. Q., Zhang, W., Chang, M. T., Lin, C. T., Chang, K. D., ... & Lin, T. W. (2012). Synthesis of Large‑Area MoS2 Atomic Layers with Chemical Vapor Deposition. Advanced Materials, 24(17), 2320-2325.Corrosion Science, 15(4), 239-250.

[56] Karbasian, H., & Tekkaya, A. E. (2010). A review on hot stamping. Journal of Materials Processing Technology, 210(15), 2103-2118.

[57] Hampden‑Smith, M. J., & Kodas, T. T. (1995). Chemical vapor deposition of metals: Part 1. An overview of CVD processes. Chemical Vapor Deposition, 1(1), 8-23.

[58] Helmersson, U., Lattemann, M., Bohlmark, J., Ehiasarian, A. P., & Gudmundsson, J. T. (2006). Ionized physical vapor deposition (IPVD): A review of technology and applications. Thin Solid Films, 513(1), 1-24.

[59] Yap, Y. K. (2012). Physical Vapor Deposition. In Encyclopedia of Nanotechnology (pp. 2069-2075). Springer Netherlands.

[60] Mattox, D. M. (2010). Handbook of physical vapor deposition (PVD) processing. William Andrew.

[61] Yerokhin, A. L., Nie, X., Leyland, A., Matthews, A., & Dowey, S. J. (1999). Plasma electrolysis for surface engineering. Surface and Coatings Technology, 122(2), 73-93.

[62] Yerokhin, A. L., Snizhko, L. O., Gurevina, N. L., Leyland, A., Pilkington, A., & Matthews, A. (2003). Discharge characterization in plasma electrolytic oxidation of aluminium. Journal of Physics D: Applied Physics, 36(17), 2110.

[63] Snizhko, L. O., Yerokhin, A. L., Pilkington, A., Gurevina, N. L., Misnyankin, D. O., Leyland, A., & Matthews, A. (2004). Anodic processes in plasma electrolytic oxidation of aluminium in alkaline solutions. Electrochimica Acta, 49(13), 2085-2095.

[64] Nie, X., Leyland, A., & Matthews, A. (2000). Deposition of layered bioceramic hydroxyapatite/TiO 2 coatings on titanium alloys using a hybrid technique of micro-arc oxidation and electrophoresis. Surface and Coatings Technology, 125(1), 407-414.

[65] Nie, X., Meletis, E. I., Jiang, J. C., Leyland, A., Yerokhin, A. L., & Matthews, A. (2002). Abrasive wear/corrosion properties and TEM analysis of Al 2 O 3

coatings fabricated using plasma electrolysis. Surface and Coatings Technology, 149(2), 245-251.

[66] Nie, X., Leyland, A., Song, H. W., Yerokhin, A. L., Dowey, S. J., & Matthews, A. (1999). Thickness effects on the mechanical properties of micro-arc discharge oxide coatings on aluminium alloys. Surface and Coatings Technology, 116, 1055-1060.

[67] Chen, Y., Nie, X., & Northwood, D. O. (2009). Plasma Electrolytic Oxidation (PEO) coatings on a zirconium alloy for improved wear and corrosion resistance.

[68] Xue, W., Deng, Z., Chen, R., & Zhang, T. (2000). Growth regularity of ceramic coatings formed by microarc oxidation on Al–Cu–Mg alloy. Thin Solid Films, 372(1), 114-117.

[69] Yu, S. X., Yuan Xia, Chen, L., Guan, Y. J., & Yao, M. (2004). Formation and structure of composite coating of HDA and micro-plasma oxidation on A3 steel.

[70] X.Z. Yang, Y.D. He, D.R. Wang, W. Gao. (2003). Al2O3 film deposited by micro-plasma oxidation on stainless steel. Chin. Sci. Bull., 48 (8), 746–750

[71] Gu, W., Shen, D., Wang, Y., Chen, G., Feng, W., Zhang, G., ... & Yang, S. (2006). Deposition of duplex Al 2 O 3/aluminum coatings on steel using a combined technique of arc spraying and plasma electrolytic oxidation. Applied surface science, 252(8), 2927-2932.

[72] Gu, W. C., Lv, G. H., Chen, H., Chen, G. L., Feng, W. R., Zhang, G. L., & Yang, S. Z. (2007). Preparation of ceramic coatings on inner surface of steel

tubes using a combined technique of hot-dipping and plasma electrolytic oxidation. Journal of alloys and compounds, 430(1), 308-312.

[73] Ma, Y., Nie, X., Northwood, D. O., & Hu, H. (2004). Corrosion and erosion properties of silicate and phosphate coatings on magnesium. Thin Solid Films, 469, 472-477.

[74] Hussein, R. O., Northwood, D. O., & Nie, X. (2012). The influence of pulse timing and current mode on the microstructure and corrosion behaviour of a plasma electrolytic oxidation (PEO) coated AM60B magnesium alloy. Journal of Alloys and Compounds, 541, 41-48.

[75] Hussein, R. O., Nie, X., & Northwood, D. O. (2013). An investigation of ceramic coating growth mechanisms in plasma electrolytic oxidation (PEO) processing. Electrochimica Acta, 112, 111-119.

[76] Hussein, R. O., Northwood, D. O., & Nie, X. (2013). The effect of processing parameters and substrate composition on the corrosion resistance of plasma electrolytic oxidation (PEO) coated magnesium alloys. Surface and Coatings Technology, 237, 357-368.

[77] Hussein, R. O., Northwood, D. O., Su, J. F., & Nie, X. (2013). A study of the interactive effects of hybrid current modes on the tribological properties of a PEO (plasma electrolytic oxidation) coated AM60B Mg-alloy. Surface and Coatings Technology, 215, 421-430.

[78] E. Bardal, Corrosion and Protection, Springer-Verlag London Berlin Heidelberg, USA, 2004.

[79] http://pixhder.com/zero+resistance+ammeter+circuit

[80] http://www1.uwindsor.ca/glier/environmental-scanning-electron-microscope-0

[81] Nie, X., Leyland, A., & Matthews, A. (2000). Low temperature deposition of Cr (N)/TiO 2 coatings using a duplex process of unbalanced magnetron sputtering and micro-arc oxidation. Surface and Coatings Technology, 133, 331-337.

[82] Zhou, X., Thompson, G. E., Skeldon, P., Wood, G. C., Shimizu, K., & Habazaki, H. (1999). Film formation and detachment during anodizing of Al– Mg alloys. Corrosion Science, 41(8), 1599-1613.

VITA AUCTORIS

NAME: Fuyan Sun

PLACE OF BIRTH: Changchun, China

YEAR OF BIRTH: 1990

EDUCATION: Jilin University, China

        2009-2013, B.Sc

        University of Windsor, Canada

        2013-2015, M.A.Sc